Aalto University
School of Science
Master's Programme in Life Science Technologies

Susanna Aro

Large-scale brain networks using MEG: pipeline and application to real data

Master's Thesis
Espoo, January 6, 2019

Supervisor: Professor Riitta Salmelin
Advisors: Mia Liljeström D.Sc. (Tech.)
Marijn Van Vliet D.Sc (Tech.)

Aalto University
School of Science
Master's Programme in Life Science Technologies

ABSTRACT OF
MASTER'S THESIS

Author: Susanna Aro

Title:

Large-scale brain networks using MEG: pipeline and application to real data

Date: January 6, 2019 **Pages:** v + 63

Major: Complex Systems **Code:** SCI3060

Supervisor: Professor Riitta Salmelin

Advisors: Mia Liljeström D.Sc. (Tech.)
Marijn Van Vliet D.Sc (Tech.)

Research has shown that functional connectivity is a powerful tool in the study of the complex processes of the human brain. Functional connectivity is generally defined as the synchronisation of anatomically distant areas and it can be inspected for example through coherent oscillations. Magnetoencephalography (MEG) is well suited for functional connectivity studies as it has a good time resolution that allows us to observe the changes in magnetic field in real time. Dynamic Imaging of Coherent Sources (DICS) uses spatial filters to estimate the oscillatory activity in the human brain.

In my master's thesis, I introduce a python-based pipeline and code library that estimates functional connectivity from MEG data using DICS. I will then demonstrate the application with a real MEG dataset. This pipeline also implements the use of canonical coherence, which provides a fast and stable way of calculating coherence between a large number of signal sources. The pipeline presented here consists of seven steps: First the data is preprocessed and the cross-spectral density (CSD) matrices are computed. Then the source space is computed and used with the CSD matrices to compute both oscillatory power and connectivity. These results are then analysed at the group-level and visualised. The results show that the pipeline is easy to apply to a real world dataset. Selection of the parameters in different steps should be made based on the dataset at hand and the results should be interpreted carefully. Further research on the stability of this pipeline is suggested.

Keywords: DICS, MEG, functional connectivity, beamformer, coherence

Language: English

Aalto-yliopisto
Perustieteiden korkeakoulu
Tietotekniikan koulutusohjelma

DIPLOMITYÖN
TIIVISTELMÄ

Tekijä: Susanna Aro

Työn nimi:
Laajat aivoverkot ja MEG: koodikirjasto ja sovellus mittausaineistoon

Päiväys: 6. tammikuuta 2019 **Sivumäärä:** v + 63

Pääaine: Complex Systems **Koodi:** SCI3060

Valvoja: Professori Riitta Salmelin

Ohjaajat: TkT Mia Liljeström
TkT Marijn Van Vliet

Toiminnallisten kytkösten tarkastelu on osoittautunut tehokkaaksi apuvälineeksi aivojen monimutkaisten toimintojen tutkimisessa. Neurotieteessä toiminnallinen kytkeytyvyys määritellään yleensä aivojen rakenteellisesti etäisten rakenteiden tahdistumisena. Toiminnallista kytkeytyvyyttä voidaan tarkastella esimerkiksi koherenssin avulla. Magnetoenkefalografia (MEG) on osoittautunut hyvän aikaresoluutionsa takia sopivaksi menetelmäksi tarkastella toiminnallisia kytköksiä. Keilanmuodostusmenetelmä koherenttien lähteiden dynaaminen kuvaaminen (Dynamic Imaging of Coherent Sources, DICS) käyttää spatiaalisuodattimia tarkastellakseen aivoissa tapahtuvia värähtelyitä.

Tässä diplomityössä esittelen python-ohjelmointikielellä toteutetun koodikirjaston, joka DICS-menetelmän avulla arvioi aivojen värähtelyjen tehoa ja koherenssia ja näin toiminnallista kytkeytyvyyttä. Tämän kirjaston DICS-menetelmässä koherenssi kahden lähteen välillä lasketaan kanonisella koherenssilla, joka on nopea ja vakaa tapa laskea koherenssi suurelle määrälle lähdepisteitä. Koodikirjaston vaiheita on seitsemän: Data esikäsitellään ja siitä lasketaan ristispektritiheysmatriisi (CSD-matriisi). Lähdepisteet määritellään ja niitä käytetään CSD-matriisien kanssa värähtelyn tehon ja yhteyksien laskemiseen. Tämän jälkeen tuloksia käsitellään ryhmätasolla ja näytetään kuvina. Tulokset osoittavat, että koodikirjaston soveltaminen mittausaineistoon on helppoa. Eri vaiheissa tarvittavat parametrit on valittava aineiston ominaisuuksien perusteella ja tuloksia on tarkasteltava varoen. Lisätutkimusta suositellaan menetelmän vakauden varmistamiseksi.

Asiasanat: DICS, MEG, toiminnallinen kytkeytvyys, keilanmuodostus, koherenssi

Kieli: Englanti

Preface

I'd like to thank my supervisors Mia Liljeström and Marijn van Vliet for giving valuable advice and help during my writing process. I'd also like to thank Jan Kujala, for his help and advice with Conpy, and Heidi Ala-Salomäki, for designing the experiment and giving me her dataset to use.

My greatest thanks to Riitta Salmelin and Imaging Language group for all these opportunities during the past few years to grow as a researcher.

And of course, thanks to the team at home, mom, dad and Juho, who have supported me through this time and proof-read the text with only a little complaining.

Espoo, January 6, 2019

Susanna Aro

Contents

Chapter 1

Introduction

The brain is an organ with billions of neurons working together to allow us to perform all the everyday functions. It is the organ that has made it possible for us to communicate, to create, to think. Throughout centuries humans have been interested in discovering how the brain functions. To measure the changes in the brain, imaging methods like magnetoencephalography (MEG) have been invented. These methods have given us an opportunity to see beyond the anatomical structures. For multiple years, the number of publications and neuroscience themed journals has been on the rise (Yeung et al. 2017). Especially in the recent decades, functional connectivity and neural networks have become an interesting topic in neuroscientific research. Functional connectivity analysis attempts to study connections between anatomically distant areas by inspecting the synchronisation of neuronal activity (Friston 2011).

To analyse functional connectivity existing imaging methods like MEG can be used. MEG measures how the magnetic fields around the brain change (Lopes da Silva 2010). Sensors are placed inside a helmet to measure the small fluctuations in the magnetic field caused by neuronal activity around the scalp. MEG provides a time resolution of milliseconds, allowing us to measure the changes in magnetic field in real time (Del Gratta et al. 2001). MEG also provides good spatial resolution that can be smaller than a cen-

timetre (Nijholt et al. 2008). In MEG the challenge is the source estimation, where we want to estimate the origin of the measured signal. This is called the inverse problem (Gross et al. 2013). Additionally, due to the fact that magnetic field extends to infinity, the signals measured by MEG sensors are always correlated to some extent, which creates additional challenges when studying connectivity (Gross et al. 2013; Lopes da Silva 2010).

There are various approaches for solving the inverse problem in the field of MEG studies (Jensen et al. 2010). One approach is beamforming, which uses spatial filters to estimate the contribution of each source (Hillebrand et al. 2005; Van Veen et al. 1988). A spatial filter aims to reduce the interfering signals outside the source and enhance the signal originating from the source of interest. Beamforming has provided stable results when the focus is on the power of oscillatory activity (Jensen et al. 2010). Dynamic Imaging of Coherent Sources (DICS) introduced by Gross et al. (2001) can be used to calculate both the power and coherence of oscillating signals. Laaksonen et al. (2008) used a filter bank of Morlet wavelets and calculated the CSD for short segments of time. This allows the inclusion of time information, allowing DICS to be used in studies with event-related designs (event-related DICS, erDICS). Different stimuli and tasks can then be used to study how the human brain operates in these context, thus possibly helping us to gain a deeper understanding about how the brain functions.

In Saarinen et al. (2015) the calculation of connectivity between multiple sources of interest, instead of just from a single source to others, is introduced. This all-to-all connectivity calculation is done using a method we call "canonical calculation of coherence", which allows fast and stable coherence calculations between a large number of source pairs. This is achieved by choosing the source orientations that maximise coherence using a discrete number of source orientations. The canonical calculation of coherence was employed together with erDICS in Liljeström et al. (2015). While there are existing DICS implementations for power mapping in neuroscience toolboxes like MNE (Gramfort et al. 2014) and FieldTrip (Oostenveld et al. 2011), at

the start of this project no published implementation of DICS for calculating all-to-all connectivity using canonical coherence existed, though it had been in use at Aalto University.

My master's thesis has two goals: First, I will describe an analysis pipeline that utilises the open-source python library, Conpy, which I took part in developing. As studying functional connectivity is important for understanding the complex processes of the brain, we consider an easy-to-use python library, that can be used to analyse connectivity on the entire cortex, to be relevant to the field of neuroscience and other researchers. In the future, we aim to merge the Conpy and the pipeline into MNE-python, a very popular toolbox for analysing MEG data, to make the pipeline even more widely available. My second goal is to apply the DICS pipeline to a dataset measured at Aalto University and discuss the application and the results. I will consider the stability of the current implementation and the important key factors that should be taken into account for good results.

In this master's thesis, I will first discuss the theory and background behind the python library and analysis pipeline in chapter 2. Then I will describe the analysis pipeline in chapter 3 and the results of applying it to the aforementioned dataset in chapter 4. In chapter 5, I will proceed to discuss the significance of these results both for the dataset and for the implementation in general. In chapter 6, I will consider the limitations of this Conpy library and the future steps that could be taken to further develop it.

Chapter 2

Background

Our pipeline and the Conpy library were developed for analysing functional connectivity between cortical areas from MEG data. In this chapter, I will first discuss the term functional connectivity in neuroscience, and then explain the key points of MEG relevant to this thesis.

2.1 Functional connectivity

In the field of neuroscience, a large part of studies has focused on locating the source of a specific function in the brain. This approach assumes that the specialised areas of the brain work together to create the desired output and that spatially distinct areas in the cortex communicate with each other. Such functional integration can be measured using statistical dependencies like correlation between measurements of neuronal activity, defined as functional connectivity (Friston 2011).

In the most basic form, the communication between neurons can be considered to be a process where a neuron sends a message along its axon and synapses to the receiving neuron(s) using existing anatomical connections (Purves et al. 2004). However, for higher brain function to be possible, the ability to integrate information flexibly from different spatial locations is essential (Sun et al. 2004). It has been shown that spatially distant neurons

synchronise their oscillations when reacting to visual stimuli (Gray et al. 1989). Singer (1999) suggests that this neuronal phase synchronisation does not arise from anatomical connectivity but, instead, results from dynamic interactions in the brain's network. Salinas et al. (2000) argues that if all neurons in a group send bursts of activation spikes that are synchronised within the group, the effectiveness of the message increases. Previous studies indicate that groups of neurons have a built-in attribute to oscillate, and this affects their sensitivity to input (Kopell et al. 2000; Burchell et al. 1998).

Coherence is considered to be a suitable measure for studying phase synchronisation (Miltner et al. 1999; Mormann et al. 2000; Sauseng et al. 2005) and it has been used as the definition of functional connectivity (Horwitz 2003). Fries (2005) introduced the communication-through-coherence (CTC) hypothesis, which argues that effective interaction between neuronal groups requires the groups to oscillate coherently and that coherence can be used to analyse cognitive flexibility.

For a neuronal group to send messages effectively to another group of neurons, the recipient group has to be excitable. This is possible if the group sending the message and the group receiving the message are phase-locked. Studies have shown supporting evidence to this theory, as coherent oscillations have been found in the γ-frequency band ($\sim$ 25 - 75 Hz) (Gray et al. 1989; Tallon-Baudry et al. 1997) and the β-frequency band ($\sim$ 20 Hz) (Tallon-Baudry et al. 1999). It also seems that these coherent oscillations may exist in lower frequency ranges (Palva et al. 2005). It follows that coherent oscillations on the cortex can be used as measure of functional connectivity and functional integration in the brain.

Coherence measures the consistency of phase-difference between two signals (Maris et al. 2007a). It is a non-parametric measure, as it is estimated directly from data (Gross et al. 2010). It is comparable to correlation, a very popular and simple measure of similarity. The disadvantage of correlation is that it is sensitive to both phase and polarity. While the mathematical definition of coherence is more complex than that of correlation, it is sensitive only

to changes in power or phase dynamics. Correlation gives us direct information about the shape and time dependency of two signals, while coherence tells more about the stability of similarity. The choice between correlation and coherence as a metric depends on the research question at hand (Guevara et al. 1996).

When calculating coherence, the time series must be transformed to the frequency domain using a wavelet transformation, fast Fourier transform or other similar method. To calculate the coherence for these transformed signals $X(f)$ and $Y(f)$, the auto-spectrum of both signals and the cross spectrum are needed:

$$\mathrm{Coh}_{xy}(f) = \frac{|P_{xy}(f)|^2}{P_{xx}(f)P_{yy}(f)} = \frac{|X(f)Y(f)^*|^2}{X(f)X(f)^*Y(f)Y(f)^*} \tag{2.1.1}$$

where Coh_{xy} is the coherence between the signals $Y(f)$ and $X(f)$, P_{xy} is the cross-spectrum of the signals $Y(f)$ and $X(f)$, P_{yy} and P_{xx} are the auto-spectra of the signals $Y(f)$ and $X(f)$. $Y(f)^*$ and $X(f)^*$ are the complex conjugates of the signals $Y(f)$ and $X(f)$.

Coherence Coh_{xy} can have values between 0 and 1. If the coherence is zero, the two signals of interest are completely unrelated. If the phase relationship of two signals remains constant as function of time, the coherence value is 1. If the value is below one and above zero, it can mean that noise exists in the system, not all inputs were taken into account or that nonlinearity exists in the system (Lessard 2005).

As with all dependency measures, coherence has its limitations. Coherence value between two signals can be affected by a common input from a third source, and therefore it may be impossible to determine the direct dependency between the two signals (Lessard 2005). As a measure of synchronisation for two signals, coherence is sensitive to changes in phase dynamics. Additionally, estimation of coherence requires the data to be stationary. Various solutions like event-related coherence and phase synchronisation can be used to allieviate these limitations (Gross et al. 2010; Srinivasan et al. 2007).

The interpretation of connectivity results needs to be done carefully and

not before statistical testing has been performed (Gross et al. 2013). However, the statistical test must be chosen with care, especially if coherence is used as a measure of connectivity. Generally, coherence is sampled, which results in a biased estimate of true population coherence. This means that smaller sample sizes lead to larger bias (Maris et al. 2007a). Connectivity analysis often inspects a large number of connections, which leads to a multiple comparison problem, where the likelihood of the null hypothesis being incorrectly rejected increases with the number of comparisons. Using multiple frequency bands also leads to multiple comparison problems if we want to test each band separately and control for the number of false positives or negatives across all frequency bands. Different approaches for statistical testing are recommended. The choice of statistical test depends on the connectivity measure and the approach used to estimate connectivity. For example, Gross et al. (2013) suggest the use of surrogate data created artificially to be compared against the measured data. Maris et al. (2007a) suggest that non-parametric statistical tests are suitable to be used with coherence.

2.2 MEG

Magnetoencephalography (MEG) is a non-invasive imaging technique which measures changes in magnetic fields. Analysis of MEG data can help us to estimate time courses of neural activity in different brain areas. Its good time resolution makes MEG a suitable method for analysing functional connectivity (Lopes da Silva 2010; Gross et al. 2010).

Neurons transfer information using electric signals. In their resting state, neurons have a negative resting membrane potential, which is typically between -40 and -90 mV. The negative potential is caused by the different ion concentrations between the cytoplasm and extracellular space. The cell membrane has different permeability to different ions, which causes the difference in ion concentrations. A stimulus that is strong enough causes changes in membrane permeability, leading to first rapid depolarisation and then

hyperpolarisation of the cell. After the hyperpolarisation the membrane permeability and thus the membrane potential return to their resting values. (Purves et al. 2004).

The electric currents are transferred from one nerve cell to another through synapses, which can be either electric or chemical. In electric synapses, the presynaptic and postsynaptic membranes are connected with intercellular channels, which allow passive current flow. In chemical synapses, the two membranes are not connected and instead neurotransmitters are released from the presynaptic neuron (Purves et al. 2004). These neurotransmitters cause changes in the permeability of the postsynaptic nerve cell's membrane. This leads to either depolarisation (excitatory response) or hyperpolarisation (inhibitory response). The flow of synaptic currents is slower than the rapid action potentials, and MEG signals are mostly caused by the synaptic current flow (Hämäläinen et al. 1993).

MEG measures only magnetic fields that have a component perpendicular to the skull, which means that the currents inside neurons must have a tangential component. As the cortex in the brain is folded, MEG measures only signals from sources in the fissures, which cause tangential fields that can be detected (Lopes da Silva 2010). The neurons with largest contribution to MEG signals are pyramidal neurons, as they typically are perpendicular to the cortical sheet of grey matter (Hämäläinen et al. 1993). They have long apical dendrites and when a large enough number of pyramidal neurons are activated simultaneously, they can generate coherent magnetic fields to be measured by MEG sensors (Lopes da Silva 2010).

These activated neurons can be modelled as a current dipole, which approximates the current flow in a small area (Hämäläinen et al. 1993). The current dipole $\boldsymbol{Q}$ approximates the localised primary current $\boldsymbol{J}_p(\boldsymbol{r})$, which together with return current $\boldsymbol{J}_v(\boldsymbol{r})$ sum to the electric current caused by neuronal activity $\boldsymbol{J}(\boldsymbol{r})$. The primary current can be defined as in Hämäläinen et al. (1993):

$$\boldsymbol{J}_p(\boldsymbol{r}) = \boldsymbol{Q}\delta(\boldsymbol{r} - \boldsymbol{r_Q}) \tag{2.2.1}$$

where the δ is the Dirac delta. The magnitude, direction and position of the current dipole source must be solved, and this in practice is done by fitting equivalent current dipole (ECD) from the measured magnetic field patterns using least-squares approach (Hämäläinen et al. 1993).

The magnetic field $\boldsymbol{B}$ in the quasi-static approximation of Maxwell's equations is defined using the primary current $\boldsymbol{J}_p(\boldsymbol{r})$ is as follows:

$$\boldsymbol{B}(\boldsymbol{r}) = \frac{\mu_0}{4\pi} \int \frac{\boldsymbol{J}_p(\boldsymbol{r}') \times \boldsymbol{R}}{R^3} \tag{2.2.2}$$

where the magnetic field is calculated at $\boldsymbol{r}$ and $\boldsymbol{R} = \boldsymbol{r} - \boldsymbol{r}'$. Using the quasi-static approximation of Maxwell equations, it can be shown that the electric current and the magnetic field are linearly related to the primary current. Solving the magnetic field from the primary current distribution is called the forward problem (Hämäläinen et al. 1993). The solution requires modelling the conductivity in the brain. The head can be approximated to be a simple sphere, which leads to results that are generally stable (Hämäläinen et al. 1993). However, Hämäläinen et al. (1989) suggest that a boundary-element model (BEM) provides more accurate results for sources in the frontal and frontotemporal areas. BEM can be used if anatomical magnetic resonance images (MRI) of the individual are available.

Magnetic fields caused by neuronal activation are very small, around 50 - 500 fT, which means that the detector needs to be sensitive to weak magnetic signals. MEG sensors use flux transformers and different sensor configurations are available. Magnetometers have a signal coil on top of the transformer and a pick-up coil closer to the brain. Gradiometers have a compensation pick-up coil that makes them less sensitive to the more distant sources. The arrangement of the coils in the sensor affects its sensitivity to the nearby sources (Parkkonen 2010; Hämäläinen et al. 1993). If we define $\boldsymbol{L}$ to be the leadfield matrix containing the sensitivity distribution of

each sensor used in measurement, there exists $\boldsymbol{L}$ that satisfies the following equation:

$$\boldsymbol{B} = \boldsymbol{LQ} \tag{2.2.3}$$

where $\boldsymbol{B}$ is the magnetic field induced by the dipole $\boldsymbol{Q}$. This equation results from the linear relation of magnetic field and the electric current to the primary current. The estimation of the leadfield is called forward modelling and it attempts to predict the magnetic field produced by a source model on a sensor level (Baillet 2010).

To localise the sources of measured MEG signals, it is necessary to coregister the measured data with anatomical information. Before the start of a MEG measurement, a set of anatomical landmarks on the subject's head are identified and then digitised, thus providing a reference frame for the functional data. The set must consist of at least three landmarks. Whalen et al. (2008) suggests that the accuracy of the alignment can be further improved with the digitisation of the whole scalp with a digiser. Coregistration to anatomical data is preferably done using subject's anatomical MRIs to achieve higher precision, but if the individual MRIs are not available templates can be used (Gross et al. 2013). Anatomical images of the brain taken with MR-scanner contain high resolution information of the tissue structures (Smith et al. 2004). A source space that contains the possible sources of interests can be constructed from anatomical images with software like Freesurfer (Dale et al. 1999; Fischl et al. 1999a). In MEG, source reconstruction is complicated by the inverse problem. The underlying current sources need to be estimated from the magnetic fields measured outside of the brain. This system is ill-defined with no unique solution (Hämäläinen et al. 1993; Baillet 2010). Fitting ECDs is a common method for solving the inverse problem (Baillet 2010).

The uncertainty in the source reconstruction leads to a phenomenon called field spread, which is caused by the fact that, theoretically, magnetic fields extend to infinity. As a result, all MEG sensors can measure it. This means

that a measured signal contains signals with multiple sources. This creates challenges especially in connectivity analysis, if we define connectivity as the dependence of two signals like in correlation. The signal mixing can, in the worst-case, result in incorrect interpretation of coherence when no actual interaction exists. Because the number of possible sources is multiple times larger than the number of sensors, there may exist a source that was not interpreted as a separate source, which in turn can affect the interpretation of observed connectivity (Gross et al. 2013). As the source localisation with multiple possible sources and noisy data is difficult, solutions like spatial filters and beamformers are used (Baillet 2010).

For dependency-based measures like correlation and coherence, it is often recommended that the connectivity analysis is performed on source level to minimise the field spread. Connectivity measures that are based on phase difference like imaginary coherence (Nolte et al. 2004) can be used to avoid incorrect interpretations caused by field spread. However, these measures may also interpret signals with neural origin as noise if they are only sensitive to phase difference. The interpretation of imaginary coherence in measurements with experimental design can be challenging as the task-related effects may cause difference in phase difference, magnitude or in both (Gross et al. 2013). Using contrasts, where two conditions are compared, while ensuring that there is no concomitant difference in oscillatory power, can reduce the effect of field spread (Gross et al. 2013).

Another common approach is to perform the connectivity analysis using specified regions of interests (ROIs), which have been selected based on prior knowledge or maps of neuronal activity. This limits the number of comparisons in the connectivity analysis. However, incorrectly selected ROIs may lead to incorrect interpretation of the underlying interactions, and even when ROIs are selected correctly field spread may still cause incorrect interpretations (Schoffelen et al. 2009).

Chapter 3

The pipeline and Conpy

As stated in chapter 1, one of the main tasks of my thesis was to implement a python-based pipeline and code library, Conpy, that uses DICS beamforming first introduced in Gross et al. (2001) to estimate oscillatory power and connectivity from MEG data. We wanted to include the modifications that were used in the studies by Saarinen et al. (2015) and Liljeström et al. (2015), and now published in van Vliet et al. (2018). The most important modification is the use of canonical coherence in connectivity analysis, which allows efficient calculations of all-to-all connectivity by selecting source orientations that maximise coherence. The original DICS presented in Gross et al. (2001) is used for coherence from one source of interest. In all-to-all connectivity, connections between multiple sources are considered. The canonical coherence will be discussed in more detail in section 3.6.

We chose to implement the pipeline using the MNE-python software (Gramfort et al. 2013; Gramfort et al. 2014). The MNE software includes a wide variety of functions to process electromagnetic data. When this project started, the DICS beamformer was also already implemented in MNE, but it did not have the functionality for calculating connectivity between all possible sources. The pipeline described here is the stable version published in van Vliet et al. (2018), where the CSD computations and power mapping have been merged into MNE-python.

Our goal is that the Conpy and the pipeline will be merged into MNE-python. We also wanted to publish the pipeline independently to guarantee that the results published in van Vliet et al. (2018) would remain replicable also in the future. The code examples here work with Conpy version 1.0 and MNE-python version 0.16.

The pipeline consists of 7 steps, which are covered in depth in this chapter. I will first discuss the theory and then demonstrate the implementation with sample code of how to use the code library. This chapter closely follows van Vliet et al. (2018). First, the measured MEG data must be pre-processed so that the analysis can be performed. Then, cross-spectral matrices are calculated for each subject. A common grid is created and morphed to each subject to allow group-level analysis. Coherence is calculated using a CSD matrix and a forward operator containing the leadfield. Group-level analysis combines the individual level results and uses statistics to remove spurious connections. These results can then be then visualised.

3.1 Dynamic imaging of coherent sources

Gross et al. (2001) introduced a method for estimating functional connectivity at the source level called Dynamic Imaging of Coherent Sources (DICS). DICS can be used to calculate both the power spectra and the coherence of oscillatory activity. As DICS uses a spatial filter, it is considered a beamforming technique.

Beamformers employ discrete spatial filtering to reduce the effect of noise and signals originating from sources outside the area of interest (Van Veen et al. 1988) and they have been used successfully in different MEG studies (Hillebrand et al. 2005; Sekihara et al. 2001; Brookes et al. 2011). Another benefit is that they do not need prior information of the number of possible sources as the spatial filter is calculated for each point in the source space. However, the source space containing the possible sources of interest must be defined, as the narrowband spatial filter is applied at each defined point.

Calculating the spatial filter for each point changes the source localisation problem into a signal detection problem (Hillebrand et al. 2005; Baillet 2010; Jensen et al. 2010).

The magnetic field resulting from neuronal activation can be represented with equation 2.2.3. For beamformers in general, Mosher et al. (2003) show that using a generalised linear solution, the current distribution of a dipole $\boldsymbol{Q}$ can be defined with the following equation:

$$\boldsymbol{Q} = \boldsymbol{C}_j \boldsymbol{L}^T \boldsymbol{C}_b^{-1} \boldsymbol{B} \tag{3.1.1}$$

where $\boldsymbol{C_j}$ is the covariance matrix for the source currents and $\boldsymbol{C_b}$ the covariance matrix for the data (Mosher et al. 2003). Now, if σ_j^2 is defined as the signal power, we have the relation $\boldsymbol{C_j} = \text{diag}(\sigma_j^2)$. The signal power σ_j^2 can then be defined using $\boldsymbol{C_j}$ as in Hillebrand et al. (2005):

$$\sigma_j(r)^2 = (\boldsymbol{L}(r)^T \boldsymbol{C}_b^{-1} \boldsymbol{L}(r))^{-1} \tag{3.1.2}$$

These two equations 3.1.1 and 3.1.2 give us the beamforming algorithm:

$$\boldsymbol{Q}(r) = \boldsymbol{A(r)}^T \boldsymbol{B} = (\boldsymbol{L}(r)^T \boldsymbol{C}_b^{-1} \boldsymbol{L}(r))^{-1} \boldsymbol{L}(r)^T \boldsymbol{C}_b^{-1} \boldsymbol{B} \tag{3.1.3}$$

where $\boldsymbol{A(r)}$ contains the weights of the spatial filter. When the orientation of the current dipole is not known, the optimal solution can be searched (Hillebrand et al. 2005). As seen from the equations 3.1.1 and 3.1.2 above, beamforming uses covariance matrices. For covariance matrices and results to be accurate, enough data must be collected. As a pre-defined source space is used, inaccuracies in the head conductor model lead to erroneous results in beamforming (Baillet 2010).

In Gross et al. (2001) oscillatory components of MEG signals are represented with the cross-spectral density (CSD) matrix with complex values instead of a covariance matrix. The cross-spectral density between signals $x(t)$ and $y(t)$ is defined as $X(f)Y(f)^*$ as in equation 2.1.1. In Gross et al. (2001) the time signal is transformed using Welch's method (Welch 1967).

However, DICS as presented in Gross et al. (2001) is best suited for continuous data due to its limited time-frequency resolution tradeoff within small time intervals (Laaksonen et al. 2008). Event-related DICS (erDICS) introduced in Laaksonen et al. (2008) included modifications that allowed more flexibility with event-related studies. Time-dependent CSDs are calculated using wavelets, resulting in better time-frequency resolution trade-off. As a result, erDICS can be used when the study has an event-related design where the tasks and stimuli appear in random order. erDICS allows the investigation of oscillatory activity around the occurrence of the stimuli. A caveat of the wavelet approach is that the time resolution is limited. Additionally, when CSDs are averaged, we assume that the source orientation remains static throughout the task. This is a common assumption in event-related approaches (Laaksonen et al. 2008).

3.2 Data pre-processing

Before our DICS library and pipeline can be applied to a MEG dataset, several pre-processing steps are necessary. Noisy or flat channels must be taken into account and artefacts caused by eye saccades and other muscle activity must be removed. For event-related DICS it is important to split the measurement data into smaller segments that are centred around the task stimuli. Here I give only a general overview of these necessary steps. Gross et al. (2013) contains more discussion and suggestions for good MEG data pre-processing. For a more detailed discussion, the reader is referred to Jas et al. (2018).

MEG measurement data often contains artefacts from movements and some channels may contain low quality data. To increase the signal-to-noise ratio, artefact removal and de-noising is needed (Jas et al. 2018). For Elekta Neuromag systems, like the device at Aalto University, the first step is the application of signal space separation (SSS) or spatiotemporal signal space separation (tSSS), both available in Elekta MaxFilter software. The software

also recognises if some sensors did not measure any data. If this step is left out, these sensors need to be identified by other means. A detailed explanation for SSS is available in Taulu et al. (2005) and for tSSS in Taulu et al. (2006).

Artefacts caused by eye blinks can be removed from the data in several different ways. Data segments with artefacts can be manually or automatically identified and left out, or artefact correction methods can be used (Gross et al. 2013). Artefact fields often have a specific distribution which can be taken advantage of to remove artefacts (Nolte et al. 1999). There are spatial filtering methods that remove noise, like Independent Component Analysis (ICA) or Signal-Space Projection (SSP). However, modifying the signal to remove artefacts has the risk that some of the signal of interest is also lost. Methods that modify the signal by removing artefact components, like SSP and ICA, are therefore best suited for cases where the number of trials is already small before artefact rejection (Gross et al. 2013).

MEG data analysis is traditionally event-related; hence the measured data is segmented and centred on the onset of the stimulus. The MEG measurement contains information of these onsets. Typically different stimuli are marked with different codes so that they can be separated in the analysis.

3.3 Cross-spectral density matrices

DICS uses cross-spectral density matrices, which must be calculated for each frequency band. In the original paper by Gross et al. (2001) discussed in section 3.1, these were calculated using Welch's method, which employs a Fast Fourier Transform (Welch 1967). We chose to use Morlet wavelets as introduced in Laaksonen et al. (2008). Their definition for Morlet wavelet is modified from Tallon-Baudry et al. (1997):

$$M(t, f_c, \sigma_t) = Se^{\frac{-t^2}{2\sigma_t}} e^{i2\pi f_c t} \tag{3.3.1}$$

where S is the scaling parameter $S = (\sigma_t\sqrt{\pi})^{-\frac{1}{2}}$. An important parameter

is the wavelet width, which is defined as the ratio between frequency f_c and the standard deviation in frequency domain σ_f, which depends on the standard deviation in time σ_t so that $\sigma_f = \frac{1}{2\pi\sigma_t}$.

This ratio controls the trade-off between the time and frequency resolution. One popular tactic is to choose better frequency resolution for lower frequencies and better time resolution for higher frequencies. If we define the wavelet width to be $n_0 = \frac{f_c}{\sigma_f}$, then the standard deviation σ_t can be defined as in Tallon-Baudry et al. (1997):

$$\sigma_t = \frac{n_0}{2\pi f_c} \tag{3.3.2}$$

To construct the Morlet wavelet with the chosen length, we define the time points to evaluate as $t = \{-5\sigma_t, -5\sigma_t + \frac{1}{f_s}, \ldots, 5\sigma_t\}$, where f_s is the sampling frequency (van Vliet et al. 2018).

Now we can define the Morlet function Eq. 3.3.1 as

$$M(f_c) = (\sigma_t\sqrt{\pi})^{\frac{1}{2}} e^{\frac{-t^2}{2\sigma_t^2}} e^{2i\pi f_c t} \tag{3.3.3}$$

The signal $x(t)$ is then transformed to a vector in the frequency domain $X(f_c)$ using the Morlet function defined above using linear combination $(*)$ Cross-spectral density between two signals $x_1(t)$ and $x_2(t)$ for frequencies of interest is then defined as:

$$c(x_1(t), x_2(t)) = \frac{1}{N_f}\frac{1}{N_t}\sum_{f_c}\sum_{t}(M(f_c) * x_1(t)) \times \overline{M(f_c) * x_2(t)} \tag{3.3.4}$$

where the $\overline{\ }$ stands for the complex conjugate. N_f and N_t are the number of frequencies and the number of time points. Equation 3.3.4 results in one (complex) cross-spectral density value between two channels. The values are complex if the signals x_1 and x_2 are distinct. The equation 3.3.4 is then repeated for each channel pair so that the result is a matrix containing the cross-spectral density value for each channel pair for frequency f_c and time

point t. This matrix is calculated for each individual data segment (single CSD) which is then averaged to get the mean CSD matrix $\boldsymbol{C}(f)$ (van Vliet et al. 2018).

The calculation of CSD matrices was available in MNE-python at the time of implementation, however there was no option to use the Morlet wavelet. This functionality is now merged into MNE (van Vliet et al. 2018). The discrete frequencies were retained in the matrix, so that the same object could be averaged for the chosen frequency band instead of saving a separate CSD object for each frequency band of interest. The time window needs to be defined beforehand to make calculations faster and to save disk space.

Below I show a code sample to demonstrate how to create the mean CSD for the selected frequency band using Conpy. The data segments ate created from the raw data and the CSD matrix is computed from the onset of the stimuli to 600 ms after the onset. Then the matrix is averaged across 17 - 25 Hz frequency range. The `decim` parameter is the decimation factor, which down-samples the signal so every 10th sample is used. This makes the computations faster and more memory efficient.

```
import conpy, mne
segments = mne.read_epochs('subject01-epo.fif')
csd = mne.time_frequency.csd_morlet(segments, frequencies, tmin=0,
                                    tmax=0.6, decim=10)
csd_alpha = csd.mean(17, 25)
```

3.4 Forward operator and source space

To form the forward operator containing the lead field, the source space must be defined. Gross et al. (2013) recommends that if anatomical MRIs are available, they should be used. In this case, MNE uses the Freesurfer software's surface functionality (Dale et al. 1999; Fischl et al. 1999a). Briefly explained, Freesurfer performs several processing steps that strip the skull from the MR images and classify whether points are white matter or not.

This segmentation is further used to create white matter surface that is based on the border of white and grey matter. Another surface created is the so-called pial surface, which follows the border between gray matter and pia.

The source space contains the locations, the source points, of elementary dipoles. If surface is used, MNE creates the source space by subsampling using a defined scheme and the surfaces between white and grey matter as default. The sensor locations need to be coregistered to the anatomical coordinates. During the MEG measurement the location of the sensor array is saved. Before the actual measurement landmarks on subjects' face and coil locations are digitized and this information is included in the measurement files. Initial approximation is done by identifying landmarks from the MRI-based head surface, after which the coregistration is optimised automatically (Gramfort et al. 2014).

When analysis is performed on group-level, the results must be comparable across the subjects. In MNE this is commonly done using surface based normalisation, where the subject's data is morphed to the average brain called "fsaverage" using Freesurfer's registration methods (Gramfort et al. 2014). This morphing transforms the source space of individual subjects to the same source space, so that the analysis results are comparable across subjects. This average brain is included in Freesurfer and it was created using MR images of 40 individuals (Fischl et al. 1999b). When calculating oscillatory power, this morphing is used. However, for group-level connectivity analysis we need the same connections to exist for all subjects to be able to compare the connections across subjects. Therefore, for each subject, the exact same points in the source space need to exist, and the connection pairs must be the same for each subject. As a result, morphing the connectivity results to the average brain is not possible. Instead, we define the source space in the average brain and morph it to the each subject. These morphed source spaces are then used for creating the forward operator for each subject.

A head conductivity model is needed to calculate the potentials and mag-

netic fields at the surface (Gramfort et al. 2014). If anatomical information is available, piecewise-constant conductivity model and Freesurfer segmentation can be used (Jas et al. 2018). In this case, BEM can be used to estimate the electric potential and magnetic field. BEM methods attempt to solve the surface potentials of electric currents using numerical methods (Mosher et al. 1999). MNE uses the linear collocation method introduced in Mosher et al. (1999) to create the BEM (Gramfort et al. 2014). The forward operator, which contains the leadfield, models each source point with ECDs using three separate orthogonal dipoles (Hämäläinen et al. 1993).

The number of source points depends on the choice of subsampling scheme selected for the source space, ranging from a little over 2000 to over 20 000 source points (Gramfort et al. 2014). Calculating connectivity for all possible pairs can therefore become computationally expensive, which is why the number of source points are restricted in the analysis. First, sources too far away from MEG sensors cannot be reliably detected, so leaving them out of the connectivity analysis should leave out only connections we cannot reliably detect. In the pipeline, the default cut-off value for the maximum distance from a source point to a MEG sensor is 7 cm. However, the cut-off value depends on the data at hand as we want to maintain enough source points to cover the cortex, but leave out enough points to make the connectivity computations feasible. The quality of this step should be checked using visual inspection. The same exact points need to be defined for every subject for connectivity analysis. This restriction is done for one subject and then the forward operators of others are restricted to the same source points. A good guideline for selecting the subject that is used for restricting the source space is to find an individual whose head position within the MEG helmet is close the average position across subjects.

Another way to reduce the computation times during the connectivity analysis is to use two ECDs instead of three. The three orthogonal dipoles in a source point are transformed into two orthogonal dipoles tangential to the spherical approximation of the head. These tangential sources generate

stronger magnetic fields than radial sources (Hämäläinen et al. 1993). We call this modified leadfield the tangential leadfield and recommend using it for connectivity. This is because computing the canonical coherence with the tangential leadfield gives stable results while reducing the computation time. Estimation of oscillatory power requires less computation time, so the use of leadfields with three dipoles is recommended (van Vliet et al. 2018).

Below is a code example modified from van Vliet et al. (2018) that shows how to restrict the source space for one subject and create the forward operator. In this example the source space is subsampled with icosahedrons, which results in 2562 source points for each hemisphere.

```
import conpy, mne
# Morph the average brain into a subject
src_avg = mne.setup_source_space('fsaverage', spacing='ico4')
src_sub = mne.morph_source_spaces(src_avg, subject='subject01')

# Leave out sources further than distance threshold away form sensors
info = mne.io.read_info('subject01-epo.fif') # Information about
sensors
verts = conpy.select_vertices_in_sensor_range(src_sub, dist=0.07,
info=info)
src_sub = conpy.restrict_src_to_vertices(src_sub, verts)

# Create a one-layer BEM model
bem_model = mne.make_bem_model('subject01', ico=4, conductivity=(0.3,))
bem = mne.make_bem_solution(bem_model)

# Create the forward operator
trans = 'sub001-trans.fif' # File containing the MRI<->Head transformation
fwd = mne.make_forward_solution(info, trans, src_sub, bem, meg=True)
# Transform to tangential
fwd_tan = conpy.forward_to_tangential(fwd)
```

3.5 Oscillatory power

As previously explained in section 3.1, DICS can be used to map oscillatory power for a given frequency band using a spatial filter. The power in the source space is calculated using the CSD matrix and the forward operator $\boldsymbol{L}(\boldsymbol{r})$. First the inverse of the CSD matrix is computed. We chose to do this with Moore-Penrose pseudoinverse (Penrose 1955) as the CSD matrix is often rank-deficient and, therefore, its inverse cannot be calculated and an approximation needs to be used. Before calculating the pseudo-inverse, the result can be made more stable by adding a small value λ to the diagonal (van Vliet et al. 2018). An important parameter for the inverse is the regularisation parameter α, which controls the sensitivity to noise. If the regularisation value is too small, the noise can dominate the power results. On the other hand, if the regularisation value is too large, even relevant details can be lost in the power map. Typical values are between 0.01 and 0.1 (van Vliet et al. 2018). Now we define the inverse of the CSD matrix as follows:

$$\lambda = \frac{\alpha \text{trace}\big(\boldsymbol{C}(f)\big)}{N_s} \tag{3.5.1}$$

$$\hat{\boldsymbol{C}}(f)^{-1} = (\boldsymbol{C}(f) + \lambda \boldsymbol{I})^{-1} \tag{3.5.2}$$

where N_s is the number of the sensors, I is the identity matrix and $(\boldsymbol{C}(f) + \lambda I)^{-1}$ is the Moore-Penrose pseudoinverse (van Vliet et al. 2018).

The leadfield can be normalised to increase its stability. Before normalisation the leadfield can favour locations close to the sensors as they affect the sensor values more. The normalisation is done by dividing the leadfield vector $\boldsymbol{L}(\boldsymbol{r}, \boldsymbol{f})$ with its norm:

$$\hat{\boldsymbol{L}}(\boldsymbol{r}, f) = \frac{\boldsymbol{L}(\boldsymbol{r}, f)}{|\boldsymbol{L}(\boldsymbol{r}, f)|} \tag{3.5.3}$$

Now we create the spatial filter for each dipole separately:

$$\boldsymbol{A}(r,f) = \frac{\hat{\boldsymbol{L}}(r,f)\hat{\boldsymbol{C}}(f)^{-1}}{\hat{\boldsymbol{L}}(r,f)\hat{\boldsymbol{C}}(f)^{-1}\hat{\boldsymbol{L}}(\boldsymbol{r},f)^{-1}} \tag{3.5.4}$$

In our approach the leadfield consists of three orthogonal dipoles, thereby we treat them as separate sources even though they are at the same location. This reduces the denominator to scalar. Equation 3.5.4 is then used to calculate the power estimates for all dipoles at the source point:

$$\boldsymbol{P}(\boldsymbol{r},f) = \boldsymbol{A}(\boldsymbol{r},f)\boldsymbol{C}(f)\boldsymbol{A}(\boldsymbol{r},f)^{T*} \tag{3.5.5}$$

The matrix contains cross-power estimates and on the diagonal are the squared power estimates for each dipole. In Gross et al. (2001) the power estimate in the dominant direction is found using the largest singular value. Other common ways to summarise the power are the sum of squared power and the squared power orthogonal to cortical surface (van Vliet et al. 2018).

The code example below shows the step for calculating the oscillatory power for one subject. The source orientation that maximises the oscillatory power by selecting the first singular value of $\boldsymbol{P}(\boldsymbol{r},f)$ is chosen.

```
import conpy, mne

# Read the forward operator and sensor information
fwd = mne.read_forward_solution('subject01-fwd.fif')
info = mne.io.read_info('subject01-epo.fif')

# Read the CSD an average for 17-25Hz band
csd = mne.time_frequency.read_csd('subject01-csd.h5')
csd = csd.mean(17, 25)

# Compute spatial filters
filters = mne.beamformer.make_dics(info, fwd, csd, reg=0.05,
                                   pick_ori='max_power')
```

```
# Get the power estimates
power = mne.beamformer_apply_dics_csd(csd, filters)
```

3.6 Connectivity

As discussed in section 2.1, the coherence between two signals can be defined using the cross-spectral density matrix. However, to be able to calculate coherence between two points on the cortex, the information contained in the leadfield needs to be included.

Gross et al. (2001) use coherence as their connectivity measure, and I discussed the benefits and caveats of coherence in section 2.1. Our pipeline deviates from the original DICS here: instead of calculating coherence as presented in section 3.1, we use "canonical coherence" as our default. Simulations done in Jalava (2009) showed that when for every source point the orientation that maximised source power was selected, there was an increase in coherence for unsynchronised sources. One way to try to avoid this is by choosing the orientation that maximises the coherence instead of the oscillatory power. This is achieved here by iterating through all the possible orientation pairs and choosing the optimal combination. The number of possible orientation pairs is often so large that this becomes computationally intensive (van Vliet et al. 2018).

Jalava (2009) suggests that instead of finding the optimal orientation pair analytically, a number of discrete tangential orientations can be used. Coherence does not depend on the direction so the possible orientations inspected need to cover only 180°. The discrete approximation is more stable and faster than analytical approach, as in practice only 50 tangential directions are needed for stable results (Jalava 2009).

We use the regularised CSD matrix defined in section 3.5 to approximate the oscillatory power, which simplifies the equation of the power estimate for one dipole r:

$$\begin{aligned}\boldsymbol{P}(r,f) &= \boldsymbol{A}(r,f)\hat{\boldsymbol{C}}(f)\boldsymbol{A}(r,f)^{T*} \\ &= \left(\frac{\hat{\boldsymbol{L}}(r,f)\hat{\boldsymbol{C}}(f)^{-1}}{\hat{\boldsymbol{L}}(r,f)\hat{\boldsymbol{C}}(f)^{-1}\hat{\boldsymbol{L}}(r,f)^{-1}}\right)\hat{\boldsymbol{C}}(f)\left(\frac{\hat{\boldsymbol{L}}(r,f)\hat{\boldsymbol{C}}(f)^{-1}}{\hat{\boldsymbol{L}}(r,f)\hat{\boldsymbol{C}}(f)^{-1}\hat{\boldsymbol{L}}(r,f)^{-1}}\right)^{T*} \\ &= \left(\hat{\boldsymbol{L}}(r)\hat{\boldsymbol{C}}(f)\hat{\boldsymbol{L}}(r)\right)^{-1}\end{aligned} \tag{3.6.1}$$

In the tangential forward operator we use two orthogonal dipoles, and the leadfield $\hat{\boldsymbol{L}}(\boldsymbol{r},\theta)$ for a source point described with two dipoles $\boldsymbol{r} = [r_1, r_2]$ as follows:

$$\hat{\boldsymbol{L}}(\boldsymbol{r},\theta) = \hat{\boldsymbol{L}}(r_1)\sin\theta + \hat{\boldsymbol{L}}(r_2)\sin\theta \tag{3.6.2}$$

Now, as suggested in Jalava (2009) the tangential orientations θ_1 and θ_2 that maximise the coherence between two source points $\boldsymbol{r}_1$ and $\boldsymbol{r}_2$ are found. This is done by iterating over a discrete number of orientations at both source points to find the optimal orientations and using the maximal coherence value (van Vliet et al. 2018):

$$\mathrm{Coh}(\boldsymbol{r_1},\boldsymbol{r_2}) = \max_{\theta_1,\theta_2}\left\{\frac{|\hat{\boldsymbol{L}}(\boldsymbol{r}_1,\theta_1)\hat{\boldsymbol{C}}(f)^{-1}\hat{\boldsymbol{L}}(\boldsymbol{r}_2,\theta_2)|^2}{\left(\hat{\boldsymbol{L}}(\boldsymbol{r}_1,\theta_1)\hat{\boldsymbol{C}}(f)^{-1}\hat{\boldsymbol{L}}(\boldsymbol{r}_1,\theta_1)\right)\left(\hat{\boldsymbol{L}}(\boldsymbol{r}_2,\theta_2)\hat{\boldsymbol{C}}(f)^{-1}\hat{\boldsymbol{L}}(\boldsymbol{r}_2,\theta_2)\right)}\right\} \tag{3.6.3}$$

To reduce the computational requirements, in section 3.4 a threshold was used to leave out sources that are too far away from the sensors, and the tangential forward operator was introduced. We also use a distance criterion that requires that for a connection to be inspected, the end points must be further apart than the selected threshold. Another purpose of the distance criterion is to reduce the effects of fieldspread discussed in section 2.2. The default threshold value is 4 cm, but a good threshold value should be chosen with care, taking into account the research question of the study (van Vliet et al. 2018).

Below is the code example how to calculate coherence for a single subject and for a single frequency band. The forward operator is first transformed to a tangential forward operator and the CSD matrix is averaged. Then, the source pairs of interest are created using the 4 cm threshold and the canonical coherence is calculated.

```
import conpy, mne

# Read the forward operator
fwd = mne.read_forward_solution('subject01-fwd.fif')
fwd_tan= conpy.forward_to_tangential(fwd)
# Read the CSD and average for 17-25Hz band
csd = mne.time_frequency.read_csd('subject01-csd.h5')
csd = csd.mean(17, 25)

# Create pairs
pairs = conpy.all_to_all_connectivity_pairs(fwd_tan, min_dist=0.04)

# Calculate connectivity
connectivity = conpy.dics_connectivity(pairs, fwd_tan, csd, reg=0.05,
                                       n_angles=50)
```

3.7 Group-level analysis

As stated in chapter 1, this pipeline is meant to be used for studies with experimental tasks. By calculating the mean difference in coherence values, contrasts for connectivity between two experimental tasks can be created across subjects. This approach identifies the parts of network where there are connectivity changes between the two experimental conditions. The use of contrasts is also a strategy to reduce the effect of field spread (Schoffelen et al. 2009).

In general, the number of connections in connectivity analysis is often quite large, making the results difficult to interpret. The large number of connections also leads to a high likelihood that coherent connections without neuronal basis are included. The challenge is to differentiate reliable connections from spurious connections. In our pipeline, this differentiation is done with statistical testing.

First, the connections are evaluated using a one-sided t-test for related samples, where the coherence values across the subjects between conditions are compared and the connections in the contrast that are above the selected p-value or t-value threshold are removed. We also assume that if the measured activity originates from physiological causes, the area of activation is larger than one source point, which is a common assumption (Bennett et al. 2009; Forman et al. 1995). If a source point with a connection is distant from other sources with connections, the likelihood that it is spurious increases. The pipeline offers two options to prune isolated connections: connections can be evaluated with distance-based hierarchical clustering or with modified version of the non-parametric clustering-permutation test introduced in Maris et al. (2007b).

When clustering is used, the connections are grouped into cluster based on their proximity using agglomerative hierarchical clustering, and only clusters with number of connections larger than a certain threshold survive. This approach controls the rate of false positives, as spurious connections are removed. In hierarchical clustering, the observations are partitioned into clusters using a similarity measure (here the Euclidean distance). In agglomerative hierarchical clustering, at the start, each object belongs to its own cluster and these clusters are then joined bottom-up using a linkage algorithm (Aggarwal et al. 2014). The important parameters for this approach are the minimum number of connections for a cluster to be accepted and the maximum distance the start and end points are allowed to vary to be considered to belong to the same cluster. This method was used to prune connections in Liljeström et al. (2015).

However, the clustering approach uses the size of the clusters as a threshold, rejecting all clusters smaller than a certain threshold. The modified non-parametric clustering-permutation test controls for false positives using randomly permuted data and assigns a p-value to each cluster. Connections close to each other and with t-values that have the same sign are grouped into the same cluster using hierarchical clustering. For every cluster, a cluster t-value is assigned by summing the absolute t-values inside the cluster. The condition labels for a random number of subjects are changed and then the largest t-values are added to a list of t-values. After the permutations have been repeated many times, only the clusters with t-value higher than 95% of the t-values created with the permutations are considered significant and others are removed. Important parameters for this function are the same distance parameter as in the agglomerative hierarchical clustering method and the initial t-value threshold. Connections with t-values smaller than the threshold (or larger than the negative threshold value) are discarded. Large clusters often have a larger cluster t-value, meaning they are more likely to be labelled significant. The important note is that the significance is for the entire cluster and does not give detailed information on how the connections inside the cluster affect the significance (Maris et al. 2007b).

Code example to how to perform the group-level analysis for three subjects is shown below. The connections are transformed to the common brain to facilitate the group-level inspection. Then the contrast is created from the grand average conditions and thresholded using two-sided t-test. Then the remaining connections are further limited using hierarchical clustering.

```
import conpy, mne

# Morph to fsaverage brain
fsaverage = mne.setup_source_space('fsaverage', spacing='ico4')
subjects = ['subject01', 'subject02', subject03']
conditions = ['task1, 'task2']
cons = dict()
```

```
for condition in  ['task1, 'task2']:
    # Go through subjects
    for subject in subjects:
        con_fname = subject + condition + 'connectivity.h5'
        con_subject = conpy.read_connectivity(con_fname)
        # Morph the Connectivity to the fsaverage brain.
        con_fsaverage = con_subject.to_original_src(fsaverage)
        cons[condition].append(con_fsaverage)

# Average the connection objects.
ga_con = dict()
for cond in  ['task1, 'task2']:
    con = cons[cond][0].copy()
    for other_con in cons[cond][1:]:
        con += other_con
    con /= len(cons[cond])  # compute the mean
    ga_con[cond] = con

# Statistics
contrast = ga_cond['task1'] - ga_cond['task2]
t, p = conpy.group_connectivity_ttest(cons['task1'],
                                      cons['task2'])
con_sig = contrast.threshold(pval, crit=p, direction='below',
                             copy=True)
con_clust = conpy.cluster_threshold(con_sig, fsaverage)
```

3.8 Visualisation

At the end of the analysis, the number of connections depends on the data, the statistical threshold and the clustering parameters. After statistical testing, there may still be even thousands of connections left. We introduce two

different ways to summarise and visualise the data to make the results easier to interpret. First, we introduce a cortical degree map. This map includes the number of connections after statistical thresholding from and to a source point. Source points with a large number of possible connections tend to have a larger number of surviving connections, making it harder to interpret the overall connectivity. The degree value may be divided by the number of connections to scale the connectivity values (van Vliet et al. 2018).

Second, we use cortical parcellations. The cortex has been divided into smaller areas, called parcels, using prior information (Fischl et al. 2004). A parcellation consists of parcels covering the entire cortex. These parcellations are provided for example in the Freesurfer software that MNE uses to create the source spaces (Gramfort et al. 2014). Each parcel contains a list of source points that belong to it (Fischl et al. 2004). The connections between two parcels are summarised using a chosen summary statistic, like the number of connections between them (”degree”), sum of the incoming and outgoing connection strengths (”sum”) or the absolute maximum value of the connections (”absmax”). There is also an option for the user to define their own summary statistic if they wish. When ”degree” or ”sum” is used, the larger parcels often have larger values, so dividing by number of possible connections can be used to reduce the bias. After the connections have been summarised to parcels, circular connectograms are used to visualise the results. A connectogram is a visualisation where the connections are visualised as a line between the connected source points, here regions. In a circular connectogram the sources are arranged in a circle. A basic visualisation can be created using a simple `connectivity_parc.plot()`, but different parameters can also be tuned to improve the interpretability and the visual appearance of the connectogram.

```
import conpy, mne

# Load thresholded connectivity contrast
connectivity = conpy.read_connectivity('contrast.h5')
```

```
# Create degree map and plot left hemisphere
brain = con.make_stc("degree", weight_by_degree=True).plot(hemi='lh')

# Read parcellation  "parcellation"  for the average brain
parcels = mne.read_labels_from_annot('fsaverage', 'parcellation')

# Summarise to parcels
connectivity_parc = connectivity.parcellate(parcellations,
weight_by_degree=True)

# Plot connectogram
connectivity_parc.plot()
```

Chapter 4

Application to real data

In this chapter the implemented DICS pipeline is applied to an existing dataset to demonstrate the functionality of our pipeline. The dataset was measured at the Aalto University, Finland and it was analysed using the steps and guidelines presented in chapter 3. This dataset is a part of another study at Aalto University Department of Neuroscience and Biomedical Engineering and it was designed to be well suited for connectivity analysis. The data was measured on two separate measurement days, allowing us to compare the similarity of the group-level results and thus discuss the stability of the pipeline described in chapter 3.

4.1 Description of the dataset

Twenty right-handed native Finnish speakers took part in two MEG measurement sessions and one MRI session. Ten subjects were male and ten female, with mean age 25.2 years (range 21 - 35 years). None of the subjects had a history of neurological disorders, psychological disorders or dyslexia. All had normal or corrected to normal vision and they consented to the experiments with prior approval of Aalto University Research Ethics committee.

The MEG experiment included four different tasks. In the "naming" task subjects were shown pictures and were asked to name the object in

the pictures out loud. In the semantic task, called "categorical", subjects answered "yes" or "no" depending on whether the object in picture was a living thing or not. There were also two visual tasks, where the subjects answered "yes" if there was a cross in the middle of the picture. In one of the visual tasks, "visual", the pictures were objects and in the other, "scrambled", task they were scrambled to make them unrecognisable. All answers were given in Finnish. The tasks were practiced before the recording sessions. The tasks were organised in five sets each consisting of 8-9 blocks. Each block contained ten pictures. There were two sessions, each consisting of 44 task blocks in a randomised order.

Four sets of pictures were used as stimuli. In the naming task and in the categorical task there were 100 pictures of objects in each session. The visual tasks had 120 pictures of which 20 were target images with a cross in the middle and were not used in the analysis. The pictures were line drawings of objects or scrambled images. Scrambled images were created from the object images and their identifiability was tested with subjects not participating in the actual MEG study. 74% of the scrambled images could not be identified. The naming agreement for objects was also assessed with subjects not participating in the actual study (22 subjects, nine males, mean age 26 years, range 19 - 33 years) and for an object to be included in the set 16 subjects had to agree on the naming. The names varied from 3 to 11 letters in length, and there were no compounds.

Categorisation between living and nonliving objects was evaluated by nine subjects that did not take part in the measurement sessions (5 males, mean age 26.7 years, age range 20 - 32 years). The number of living and nonliving objects was the same in the three tasks where objects were used. There was no statistical difference between the picture sets in naming agreement, categorisation agreement, word length or word frequency (Kruskal-Wallis test, $p > 0.05$ (Kruskal et al. 1952)). There was no significant difference between any sets in luminance (one-way ANOVA, $p > 0.05$).

MEG was recorded using a Vectorview whole-head MEG (Elekta Oy,

Helsinki Finland) with 306 channels. For blink rejection, vertical and horizontal electro-oculograms (EOG) were recorded. Mouth movements were monitored with electromyogram (EMG) and speech responses were collected. Indicator coils were placed so that the position of the head in relation to the MEG sensor array could be determined. One subject was left out during the analysis as they had too many incorrect answers in one task.

4.2 Applying the pipeline

First the measurement data was processed with the Elekta Maxfilter software package. tSSS was applied to remove artefacts in the data and transformed it the head position to be same in both measurements (Taulu et al. 2006). The effect of eye blinks was further reduced using fastICA (Nolte et al. 1999). Epochs were created using trials with correct answers from -0.4 to 1.2 s relative to onset of the stimulus. The quality of the artefact removal was then visually checked, and epochs with remaining artefacts were left out of the analysis. The number of epochs for each day across conditions was then equalised. The Freesurfer pipeline was used to create the cortical surfaces from the anatomical MRIs, and a boundary-element model was created for the forward operator (Dale et al. 1999; Fischl et al. 1999a).

For computations of oscillatory power and connectivity analysis, frequency bands of interest were defined as 17 - 25 Hz (high β), 31 - 45 Hz (low γ) and 60 - 90 Hz (high γ). The choice of frequency bands mostly follows Liljeström et al. (2015) but a larger low gamma band was chosen as evidence of coherent oscillations has been found in these frequencies (Palva et al. 2005). Averaged CSDs were computed in the 0 - 600 ms time range for each condition. Additionally a "baseline" CSD was calculated using data in the -200 - 0 ms time range. This was done to create a baseline for subject's brain activity, so that task-related effects could be compared to the state where the subject is not performing a task. In the power and connectivity analysis, the CSD matrix was averaged for each frequency band of interest.

For power and connectivity results I will mainly focus on the 17 - 25 Hz frequency band and the contrast "naming vs visual". Based on the experimental design, the "naming" condition was expected to differ from the "visual" condition.

To inspect the stability of the CSD matrices, the CSD matrices for each subject and for each measurement day were calculated for the "naming" condition and for each data segment. The CSDs for one task should be similar across the measurement days. Then, 80% of these single-trial CSDs were sampled without replacement and averaged. The sampling was repeated 1000 times. After this step, all subjects had 1000 mean CSDs for the "naming" condition for each measurement day. We focused on only the real-valued sensor power as the computations for oscillatory power discard the complex part. This also makes the visualisation and the use of statistics easier. The similarity of the sensor power between the two days was compared with Pearson's correlation coefficient, which is a quantitative measure of linear correlation (Hauke et al. 2011). Instead of just three frequency bands, the frequency bands were selected so that they covered frequencies from 3 to 90 Hz to detect also changes in the correlation coefficient outside of the chosen frequency bands. The mean correlation coefficient values between the two measurement days for randomly sampled CSDs can be seen in figure 4.1.

The correlation coefficients for within the same day were larger than the correlation coefficients between the two days across frequency bands an subject in at least 99% cases, when comparing the randomly sampled mean CSDs with each other for each subject. When the CDSs were compared between the two measurement days, the correlation coefficient varies markedly between subjects in different frequency bands, as the smallest mean correlation coefficient value is 0.48 (figure 4.1c). This implies that the CSDs for the "naming" task are not similar on the first and second measurement day for all subjects. Some subjects have mean correlation coefficient value higher than 0.90 in all frequency bands, and for others the mean correlation coefficient varies in the different time windows.

The "fsaverage" brain was morphed into each subject to allow group-level analysis. This morphed source space with 5124 source points on the cortex was used to create the forward operator for each individual and for each measurement day. For one subject, the source locations in the forward operator further than 7 cm away were left out to limit the number of possible connections. We visually confirmed that the remaining source locations covered the entire cortex. From the remaining source locations, source pairs were created for all-to-all connectivity so that all pairs were at least 4 cm apart from each other. The forward operators were restricted to contain the same source locations. When oscillatory power was calculated, no source locations were left out.

Power estimates were calculated for each subject and for each day. The results were summarised by selecting the source orientation that maximised the power. Group-level estimates were computed by taking the average of the data across subjects. Contrasts between two conditions were formed by calculating the difference between group-level conditions and dividing by the baseline. The resulting group-level contrasts "naming vs visual" (17 - 25 Hz, 0 - 600 ms) for each day can be seen in figure 4.2. Visual inspection of the power results shows that the results for the separate days appear similar in that some of the areas with oscillatory power detect are same for both days. Positive (red) values indicate that the group-level power estimate for the naming condition is larger than for the visual condition, and negative values (blue) indicate that the power estimate for the visual condition is stronger. The strength of the contrast differs between the days, but the locations are similar.

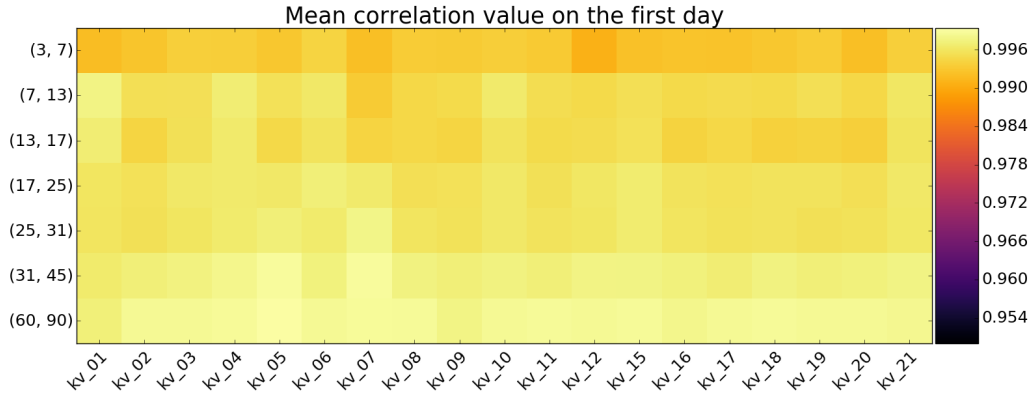

(a) The mean Pearson correlation coefficients for the first measurement day.

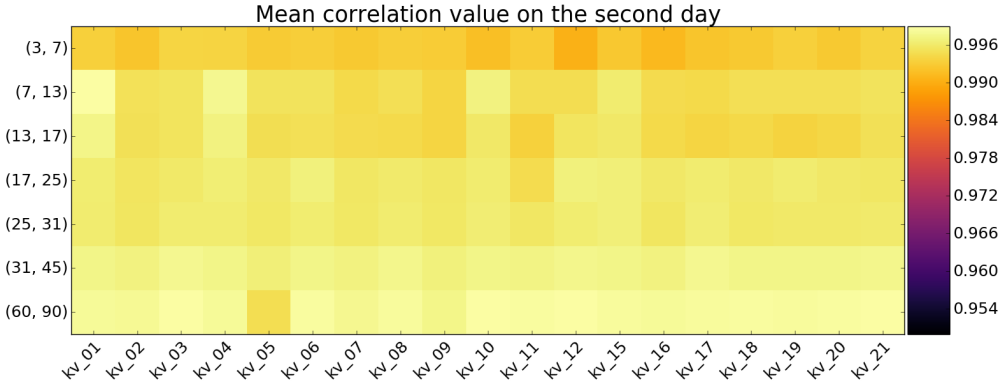

(b) The mean Pearson correlation coefficients for the second measurement day.

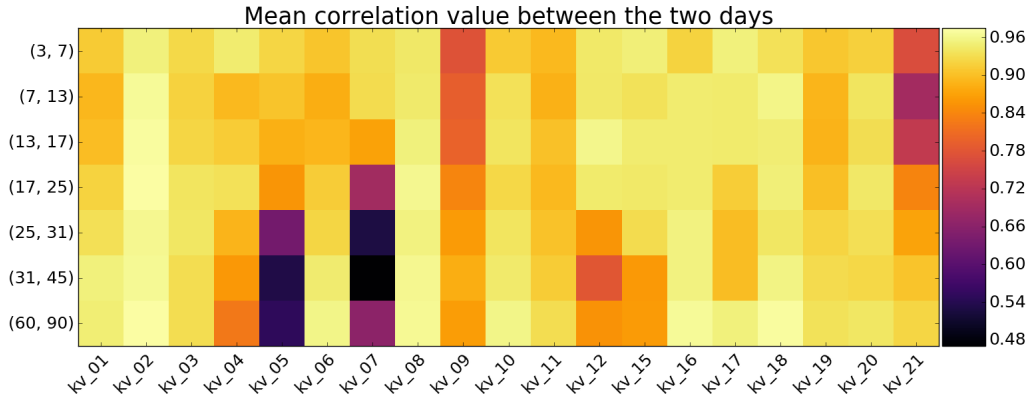

(c) The mean Pearson correlation coefficients between the first and second measurement day.

Figure 4.1: The mean Pearson correlation coefficients for the randomly sampled mean CSD diagonals for the "naming" task.

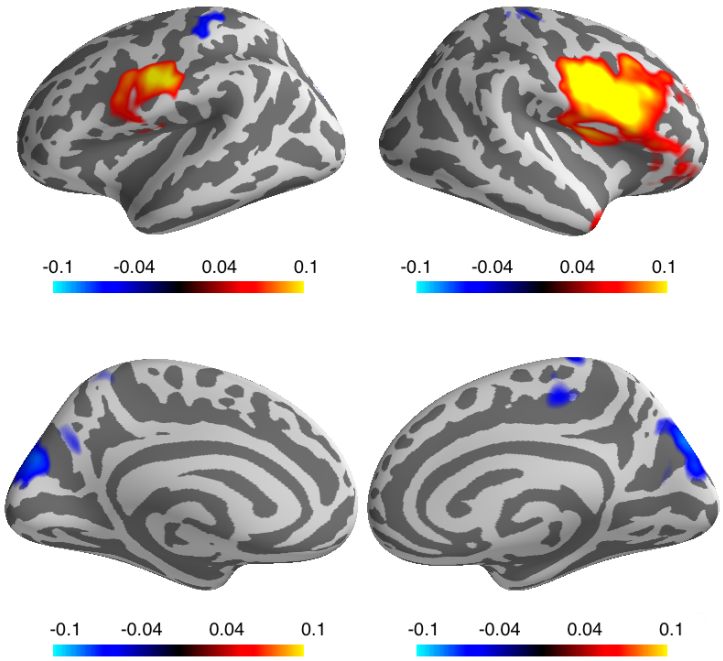

(a) Group-level power results for the first measurement day.

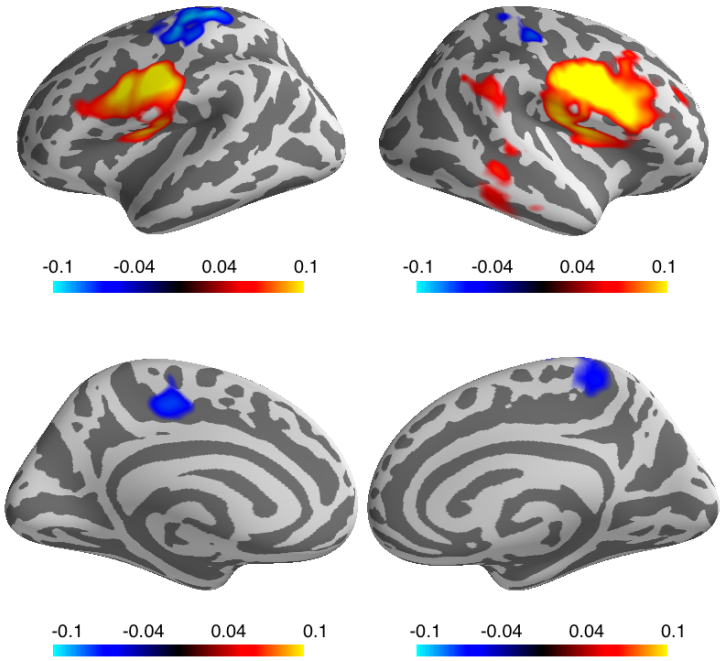

(b) Group-level power results for the second measurement day.

Figure 4.2: Group-level power results for the "naming vs visual" contrast in the 17 - 25 Hz frequency band and 0 - 600 ms time range. The contrast values were divided by the baseline condition.

The subject-level connectivity was computed for each condition for each day and each frequency band. To compare the similarity of the connectivity results between the two days, for each subject, Pearson's correlation coefficient was calculated between the coherence values of two measurement days. The correlation coefficient was computed for each frequency band of interest and for each condition. The subject-level Pearson correlation coefficients are presented in figure 4.3. The coefficient values were calculated for the coherence values between the source pairs. The subject-level correlations show that for some subjects, the conditions have a high correlation coefficient. For frequency band 17 - 25 Hz and the condition "naming" in figure 4.3a, 11 out of the 19 subjects have Pearson correlation coefficient value larger than 0.9, and the smallest value is 0.85. Additionally, the same subjects have smaller coefficients across all three frequency bands. In the 60 - 90 band (figure 4.3c), the coefficient values are higher than in the 31 - 45 Hz or 60 - 90 Hz band for most of the subjects. The largest correlation values can be found in the 60 - 90 Hz band. Subject kv_21 is an exception, performing best in the 31 - 45 Hz band and having the lowest values in both low gamma and high gamma band.

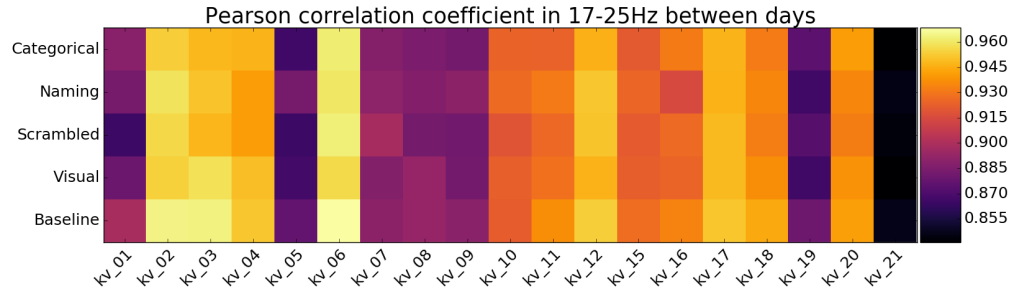

(a) Pearson's correlation coefficient for frequency band 17 - 25 Hz.

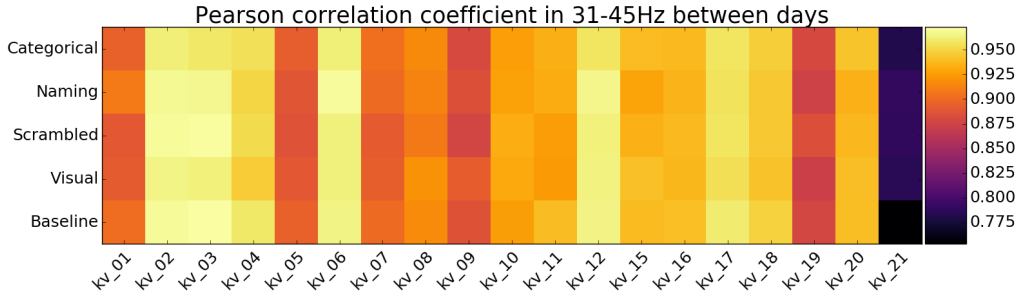

(b) Pearson's correlation coefficient for frequency band 31 - 45 Hz.

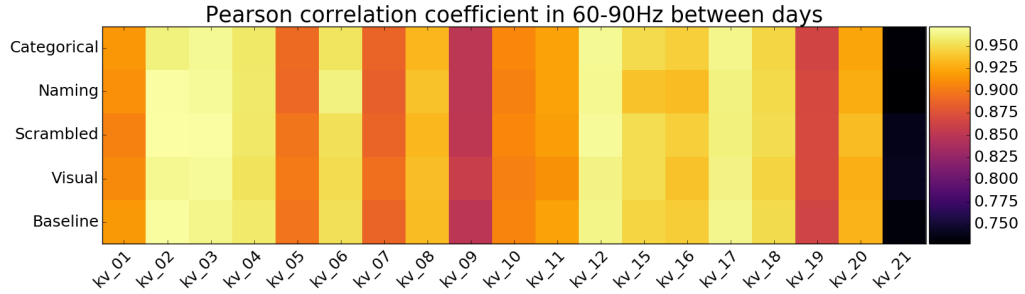

(c) Pearson's correlation coefficient for frequency band 60 - 90 Hz.

Figure 4.3: Pearson's correlation coefficient for the coherence values for each subject and each condition between the measurement days. The values were calculated for the three frequency bands of interest the time window 0 - 600 ms.

In the group-level analysis, the Pearson correlation coefficient was calculated for the mean coherence values of the source pairs across all subjects, for each condition. The results are shown in figure 4.4. Then the signed mean difference between the "naming" and "visual" conditions across subjects was computed. Two-tailed t-test for related samples was used to calculate the t-value and p-value for the "naming" vs "visual" contrast, and connections with $p \geq 0.0005$ or larger were removed. These contrasts were clustered using hierarchical clustering so that only clusters with size of at least 20 connections survived. Thresholding was done to remove spurious connections from the data. For the visualisation with a circular connectogram, the cortex was first parcellated using the Destrieux parcellation provided in the Freesurfer software (Destrieux et al. 2010). This parcellation was modified so that the average surface area of each parcel was 110 mm^2 , as shown figure 4.5.

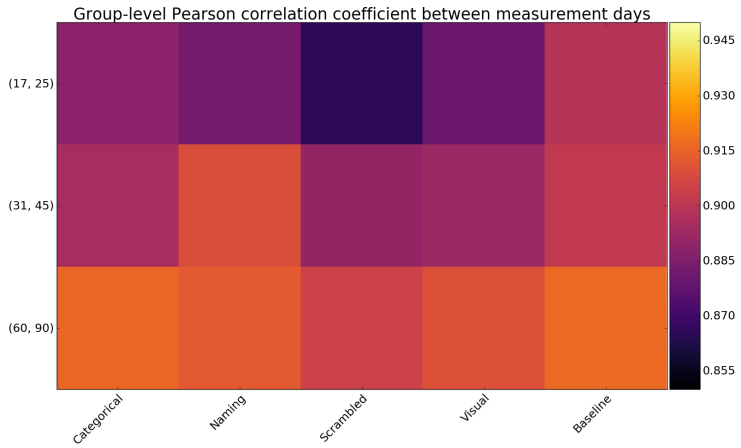

Figure 4.4: Pearson's correlation coefficient for the group-level coherence values between the source pairs in the time window 0 - 600 ms.

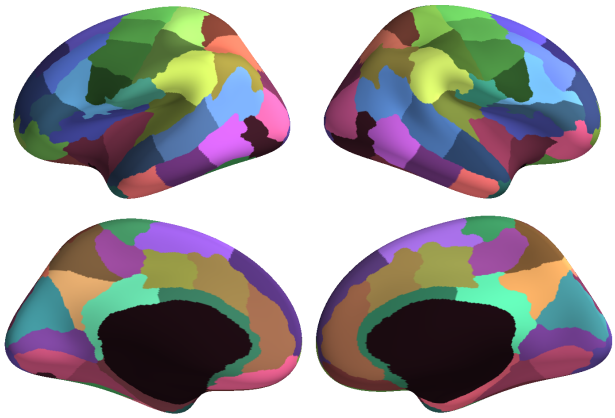

Figure 4.5: Parcellation scheme used for summarising connectivity for visualisation. Regions not included are marked in black.

These thresholded contrasts on the parcellated cortex were then visualised using circular connectograms. Additionally, the number of connections from each source point was computed and visualised in a degree map. To see how the choice of statistical threshold affected the connectivity results, the connectograms were also thresholded using p-value 0.005. The connectograms are shown in figure 4.6. The degree maps are shown in figure 4.7. The degree maps share sources that had significant connections and the locations of the sources are often the same or close by. However, the degree-map for the second measurement day contains more sources than the one for the first. Some sources that exist in the degree-map for one day, did not survive the statistical testing and clustering in the other.

To compare the similarity of the connectograms, the Jaccard index between the two days was calculated. Jaccard index is defined as the size of the intersection of two sets divided by the size of union of the two sets (Real et al. 1996). Here the intersection is the pairs that remain in both connectivity patterns, and the union is the pairs that appear only in one connectivity pattern. No weighting was used. To calculate the p-values for the results, the same number of pairs as in the connectogram was randomly sampled

from all possible pairs 1000 times and for each contrast. The p-value was calculated as the percentage of Jaccard indices of randomly sampled pairs higher or equal to the measured Jaccard index. The Jaccard indices for the contrasts thresholded with p=0.0005 are in table 4.1. The Jaccard indices for the contrasts for p=0.005 are in 4.2.

The group level connectivity results show that that the connectograms for the two measurement days (Fig. 4.6a) do not share all the same connections, and for all contrasts and all frequency bands the Jaccard index is small (table 4.1). Only "naming vs scrambled" has a significant Jaccard similarity index value ($p \leq 0.05$) in all the frequency bands, but each contrast has a significant Jaccard index in at least one of the frequency bands.

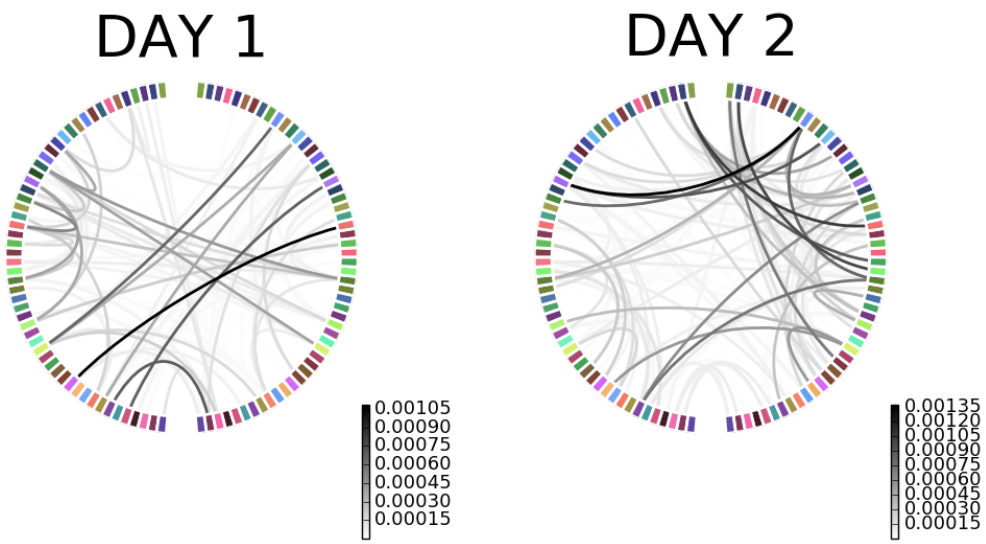

(a) Connectograms for the "naming vs visual" contrast, p=0.0005.

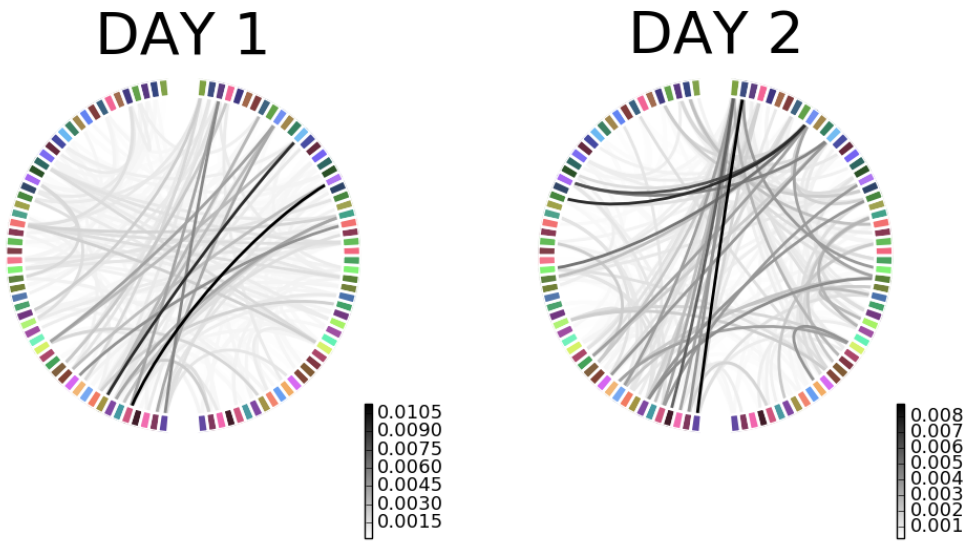

(b) Connectograms for the "naming vs visual" contrast, p=0.005.

Figure 4.6: Group-level connectivity results for the 17 - 25 Hz frequency band for first and second measurement day, cluster threshold = 20. The scale is the number of existing connections between two labels, divided by the number of possible connections between the labels.

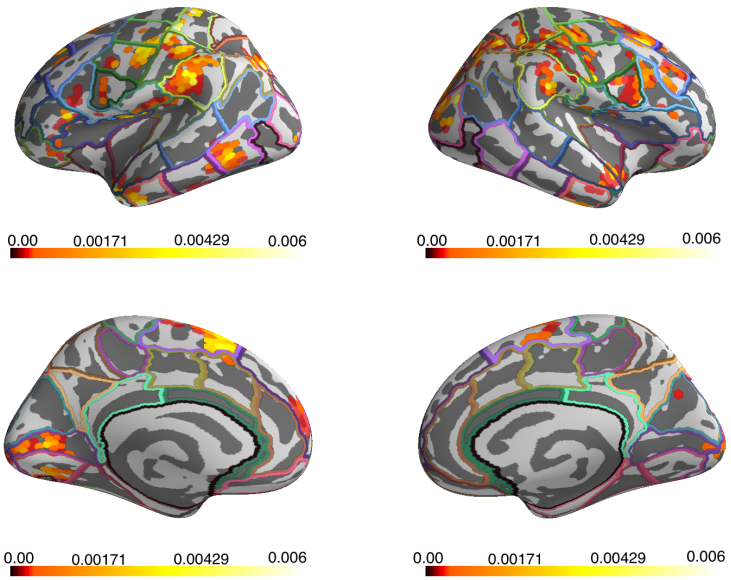

(a) The degree map for "naming vs visual" contrast for the first day.

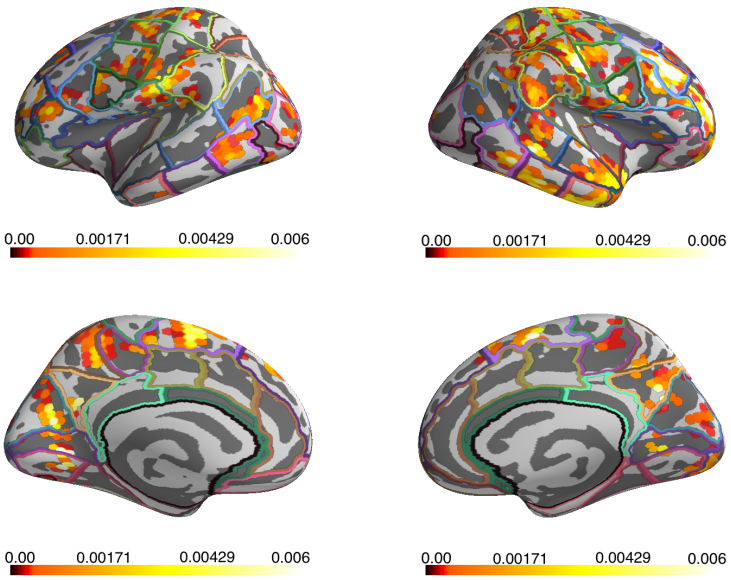

(b) The degree map for "naming vs visual" contrast for the second day.

Figure 4.7: The group level degree maps or the 17 - 25 Hz frequency band for first and second measurement day, p=0.0005 and cluster threshold = 20. The scale is defined as the number of connections for a source, divided by the number of possible connections of that source.

Table 4.1: Jaccard index for the connectograms (p=0.0005, cluster threshold 20) in the frequency bands of interest. Jaccard index is reported with 4 floating point precision and the p-values are rounded to one significant number.

Frequency band	**First condition**	**Second condition**	**Jaccard index**	**p-value**
17 - 25 Hz	Categorical	Naming	0.0714	0.0009
	Categorical	Scrambled	0.0360	0.003
	Categorical	Visual	0.0297	0.01
	Naming	Scrambled	0.0306	0.04
	Naming	Visual	0.0185	>0.05
	Scrambled	Visual	0.0236	>0.05
31 - 45 Hz	Categorical	Naming	0.0316	0.005
	Categorical	Scrambled	0.0083	>0.05
	Categorical	Visual	0	>0.05
	Naming	Scrambled	0.0374	0.02
	Naming	Visual	0.0398	0.007
	Scrambled	Visual	0.0061	>0.05
60 - 90 Hz	Categorical	Naming	0.0078	>0.05
	Categorical	Scrambled	0.0241	>0.05
	Categorical	Visual	0.0313	0.01
	Naming	Scrambled	0.0714	0.001
	Naming	Visual	0.0429	0.001
	Scrambled	Visual	0.0050	0.01

Table 4.2: Jaccard index for the connectograms (p=0.005, cluster threshold 20) in the frequency bands of interest. Jaccard index is reported with 4 floating point precision.

Frequency band	**First condition**	**Second condition**	**Jaccard index**	**p-value**
17 - 25 Hz	Categorical	Naming	0.2131	<0.001
	Categorical	Scrambled	0.2295	<0.001
	Categorical	Visual	0.1970	<0.001
	Naming	Scrambled	0.2629	<0.001
	Naming	Visual	0.2273	<0.001
	Scrabled	Visual	0.2118	<0.001
31 - 45 Hz	Categorical	Naming	0.1511	<0.001
	Categorical	Scrambled	0.1607	<0.001
	Categorical	Visual	0.1765	<0.001
	Naming	Scrambled	1	<0.001
	Naming	Visual	1	<0.001
	Scrabled	Visual	0.1549	<0.001
60 - 90 Hz	Categorical	Naming	0.1638	<0.001
	Categorical	Scrambled	0.1878	<0.001
	Categorical	Visual	0.2140	<0.001
	Naming	Scrambled	0.2817	<0.001
	Naming	Visual	0.2430	<0.001
	Scrabled	Visual	0.1556	<0.001

Chapter 5

Discussion

My two goals in this thesis were to introduce a code library and a pipeline that is based on the DICS method and to demonstrate its functionality with a real MEG dataset. I have now discussed the pipeline available in the Conpy library in chapter 3 and shown how it can be applied in chapter 4. Here I will discuss the results shown in chapter 4. Then, I will use these results to discuss the current state and future of the pipeline.

As stated in chapter 4, the randomly sampled CSDs from the same measurement day are very similar (figures 4.1a and 4.1b), which implies that the CSDs for the naming task are stable. However, the comparison between the two measurement days shows variation in the Pearson correlation coefficient. This may be due to artefact removal: if it has been more successful for one measurement day than for the other, it may affect the similarity results. However, if there were noisy data segments in the data of one measurement day, it should also affect the correlation coefficients in the within-day comparisons. Subject may also have performed differently during the two measurement days. Research has suggested that different factors like sleep deprivation (Dinges et al. 1997) and stress (Warm et al. 2008) can affect subject's performance. Additionally, the performance can be affected by non-physiological factors like personality characteristics (Rose et al. 2002).

The power results (figure 4.2) would suggest that the source level power

estimates are stable, as we have located the same areas with strongest differences for both days. However, the power results of the two measurement sessions are not identical. Larger differences are visible in the connectivity results. The variance between subjects and the high correlations within subjects may indicate that the difference in group-level connectivity results is caused by differences between the subjects. The differences in the subject-level correlations could also explain the correlation values for the group-level comparison in figure 4.4. The degree-maps share some of the sources but are not identical (figure 4.7). The differences may be due to spurious connections that were not successfully removed or result from the difference between the CSD matrices.

If the assumption is that the artefact removal has been successful, these results imply that some subjects did not perform the same in the two separate measurements. The other explanation for the difference between the two measurement days is that the pipeline described in this thesis is not stable. The results may also be affected by the low number of samples.

For this dataset, there are several different approaches that can be taken to attempt to pinpoint the cause of the differences. First, randomly sampling all other tasks could be used to attempt to explain the differences in the contrasts: if only the "naming" task is stable, it would possibly lead to differences in contrast level results. Another analysis approach, like minimum norm estimates (Gramfort et al. 2014), could be used for comparison. If the other analysis approach leads to unstable results, this would imply that the data itself is unstable. The data segments from the separate days could be averaged together to sample 80% of them 1000 times. If the pipeline results from these randomly sampled data segments are stable, the reason for the differences may be that we have too few samples in each condition. In this scenario joining the data from the two measurement days together would create more stable results.

Based on the similarities in sensor power within one measurement day, the CSD calculation can be considered stable as the CSDs calculated from

the same data have correlation coefficient higher than 99% on average. This could imply that the difference in group level results between the two measurement days is not caused by the CSD calculations, but instead from other factors like instability in the later steps in the pipeline or intra-subject differences. However, it is important to note that these results apply only for the "naming" task. The next step would be to calculate the CSD similarity for the randomly sampled CSDs for all other conditions to see if they result in comparable similarity values. Additionally, here we focused only on the diagonal values with the sensor power. Consequently, there might be larger variation outside the diagonals, which could have an effect on the connectivity results.

The differences outside of the diagonal may explain the results for subject kv_21, who has Pearson coefficient 0.9492 for the CSDs, but the correlation between the connectivity results in the same band is below 0.75. The differences can result from imperfect preprocessing, meaning that some artefacts remain in the data for one day but not in the other. Subject kv_21 does, however, have lower similarity values than the other subjects.

The variation in the p-values for Jaccard indices (table 4.1) may imply that the connectivity results are unstable. However, each contrast that includes "categorical" or "naming" condition is significant in either the 17 - 25 Hz or 31 - 45 Hz frequency band. Thus the task-related effects for these two conditions may be more stable in these two frequency bands and not others. The instability in the other frequency bands could be due to the task-related effects being too weak. For comparison, the results for p=0.005 with the same clustering threshold contain a larger number of connections and have significant and markedly larger Jaccard indices across all the frequency bands and for all conditions. However, the connections that survive the thresholding with p=0.005 do not survive the stricter p=0.0005 threshold. This implies that the shared connections in the connectograms for p=0.005 are not stable enough to survive stricter thresholding. One possibility is that the p-value 0.0005 is too strict and connections with true physiological cause are also

removed.

On the group level the conditions have large correlation values (above 0.8, figure 4.4) in each frequency band as the average across all subjects is calculated. Therefore, one cause for the differences in connectograms can be the computation of the signed mean difference between conditions, as the group level results for each condition appear relatively stable. Taking the difference may lower the similarity between the two measurement days, and the variations within and between subjects in statistical testing then further reduce the similarity. This further supports the theory that the group-level results are not similar enough to survive the statistical thresholding. Pearson correlation coefficient assumes that the relationship between the two measures is linear, which can lead to misleading results. However, Pearson correlation coefficient is used to measure the strength of the variables' relationship, making it suitable for this master's thesis (Hauke et al. 2011). Additionally, the choice of a suboptimal interaction metric would not explain the differences that result when comparing two group-level conditions.

There is also the possibility that the reason for the difference between the measurement days is caused by preprocessing. This would mean that the results using this pipeline depend on the steps performed before the application. While preprocessing is an important step in MEG, different results caused by small differences in the preprocessing pipeline would imply that the pipeline is not stable. Therefore, the next step for this pipeline should be inspecting how sensitive the pipeline is to the preprocessing. Making small changes in the preprocessing parameters and applying the pipeline again after confirming that the preprocessing appears successful could yield more information about the stability of the implementation. Large changes in the results would imply sensitivity to the choices made in preprocessing step. This can in turn cause misleading interpretation from the results.

I discussed some of the caveats of coherence as interaction metric in section 2.1. Signal mixing caused by field spread appears as phase difference of 0° or 180°, so the spurious connections caused by the field spread could

be avoided with the use of the imaginary part of the coherence. However, this also makes coherence insensitive to the couplings with zero phase with true physiological causes. Additionally, interpretation of imaginary coherence when comparing two conditions is challenging (Gross et al. 2013). This is why we chose to use coherence instead, and chose to reduce the effect of field spread by inspecting only connectivity pairs further than the threshold (here $\geq$ 4cm).

The canonical calculation of coherence attempts to find the orientations that maximise the coherence. As suggested by Jalava (2009), only a discrete number of tangential combinations are considered and the radial sources are ignored to reduce the computational requirements. This approach results in stable estimates and is well suited for studies where we are interested in differences between experimental conditions. However, another criterion for source orientation selection may be more suited, if we wish to estimate absolute coherence. Our approach to optimise the source orientation for each condition separately makes the solution less likely to prefer the condition with less noise. However, using CSD across all conditions would maximise the likelihood of field spread effects being removed in the contrasting step (van Vliet et al. 2018).

Merging Conpy into MNE allows further development of the code to make the implementation even more stable, usable and computationally efficient. For example, implementing scaling that allows the use of magnetometers in addition to gradiometers increases the amount of signal data we can use in the computation. More options in different steps of the pipeline would give the users more opportunities to use the included functions so that it is best suited to their data and research question.

Chapter 6

Conclusions

In this thesis I have introduced the Conpy library and a pipeline that allows us to map the oscillatory activity on cortical surface through power and coherence. We have introduced an implementation of canonical calculation of coherence, which finds the source orientations that maximise the coherence value between two ECDs. This is a computationally fast way of gaining stable connectivity results and allows the study of all-to-all connectivity with the DICS beamformer. The statistics and parcel-level analysis make it easier for researchers to interpret the results on different levels, from source points to larger parcels.

The aim of this project was to make a pipeline that is straightforward to use, with clear instructions and examples, so that all interested researchers would be able to use it. Integrating this pipeline into a widely known MEG data analysis toolbox allows us to reach a wider audience and to increase the usability of this pipeline even further. The source code for this project was made available so that other researchers interested in using DICS beamformer could easily also develop it further to suit their own needs and research interests of the scientific community. Releasing the source code also means that our instructions will apply even if the functionality integrated in MNE changes in the future.

I have discussed the mathematics behind this approach and shown the

necessary steps of how to use this pipeline. I have shown how the pipeline can be applied to a real world dataset and discussed the results of this application. The dataset was well suited for this pipeline, as the same subjects took part in the same experiment on two separate days. The contrasted connectivity results imply that the oscillatory activity and connectivity differ between the experimental tasks. From the connectivity results we conclude that, for this particular dataset, the results for two measurement days differ, but the sensor power and oscillatory power results imply that this is not caused by the pipeline alone. Care should be taken on how to interpret the results, and many parameters like minimum threshold between connectivity pairs should be chosen based on the dataset at hand.

Bibliography

Aggarwal, C. C. & Reddy, C. K. (2014). *Data clustering : algorithms and applications*. Boca Raton, Florida: Taylor and Francis Group, pp. 100–101. 652 pp. ISBN: 9781466558229.

Baillet, S. (2010). "The Dowser in Fields: Searching for MEG Sources". In: *MEG: An Introduction to Methods*. Ed. by Hansen, P. & Kringelbach, M. & Salmelin, R. London: Oxford University Press, pp. 83–123. ISBN: 978-0-19-530723-8.

Bennett, C. M. & Wolford, G. L. & Miller, M. B. (2009). "The principled control of false positives in neuroimaging". In: *Social cognitive and affective neuroscience* 4.4, pp. 417–422.

Brookes, M. J. & Woolrich, M. & Luckhoo, H. & Price, D. & Hale, J. R. & Stephenson, M. C. & Barnes, G. R. & Smith, S. M. & Morris, P. G. (2011). "Investigating the electrophysiological basis of resting state networks using magnetoencephalography". In: *Proceedings of the National Academy of Sciences of the United States of America* 108.40, pp. 16783–16788. DOI: 10.1073/pnas.1112685108.

Burchell, T. R. & Faulkner, H. J. & Whittington, M. A. (1998). "Gamma frequency oscillations gate temporally coded afferent inputs in the rat hippocampal slice". In: *Neuroscience Letters* 255.3, pp. 151–154. DOI: 10.1016/S0304-3940(98)00676-4.

Dale, A. M. & Fischl, B. & Sereno, M. I. (1999). "Cortical surface-based analysis: I. Segmentation and surface reconstruction". In: *NeuroImage* 9.2, pp. 179–194. DOI: 10.1006/nimg.1998.0395.

Del Gratta, C. & Pizzella, V. & Tecchio, F. & Romani, G. (2001). "Magnetoencephalography - a noninvasive brain imaging method with 1 ms time resolution". In: *Reports on Progress in Physics* 64.12, p. 1759. DOI: 10.1088/0034-4885/64/12/204.

Destrieux, C. & Fischl, B. & Dale, A. & Halgren, E. (2010). "Automatic parcellation of human cortical gyri and sulci using standard anatomical nomenclature". In: *Neuroimage* 53.1, pp. 1–15. DOI: 10.1016/j.neuroimage.2010.06.010.

Dinges, D. F. & Pack, F. & Williams, K. & Gillen, K. A. & Powell, J. W. & Ott, G. E. & Aptowicz, C. & Pack, A. I. (1997). "Cumulative sleepiness, mood disturbance, and psychomotor vigilance performance decrements during a week of sleep restricted to 4–5 hours per night". In: *Sleep* 20.4, pp. 267–277. DOI: 10.1093/sleep/20.4.267.

Fischl, B. & Sereno, M. I. & Dale, A. M. (1999a). "Cortical surface-based analysis: II: inflation, flattening, and a surface-based coordinate system". In: *Neuroimage* 9.2, pp. 195–207. DOI: 10.1006/nimg.1998.0396.

Fischl, B. & Sereno, M. I. & Tootell, R. B. & Dale, A. M. (1999b). "High-resolution intersubject averaging and a coordinate system for the cortical surface". In: *Human Brain Mapping* 8.4, pp. 272–284. DOI: 10.1002/(SICI)1097-0193(1999)8:4<272::AID-HBM10>3.0.CO;2-4.

Fischl, B. & Van Der Kouwe, A. & Destrieux, C. & Halgren, E. & Ségonne, F. & Salat, D. H. & Busa, E. & Seidman, L. J. & Goldstein, J. & Kennedy, D., et al. (2004). "Automatically parcellating the human cerebral cortex". In: *Cerebral Cortex* 14.1, pp. 11–22. DOI: 10.1093/cercor/bhg087.

Forman, S. D. & Cohen, J. D. & Fitzgerald, M. & Eddy, W. F. & Mintun, M. A. & Noll, D. C. (1995). "Improved assessment of significant activation in functional magnetic resonance imaging (fMRI): use of a cluster-size threshold". In: *Magnetic Resonance in Medicine* 33.5, pp. 636–647.

Fries, P. (2005). "A mechanism for cognitive dynamics: neuronal communication through neuronal coherence". In: *Trends in Cognitive Sciences* 9.10, pp. 474–480. DOI: 10.1016/j.tics.2005.08.011.

Friston, K. J. (2011). "Functional and effective connectivity: a review". In: *Brain Connectivity* 1.1, pp. 13–36. DOI: 10.1089/brain.2011.0008.

Gramfort, A. & Luessi, M. & Larson, E. & Engemann, D. A. & Strohmeier, D. & Brodbeck, C. & Goj, R. & Jas, M. & Brooks, T. & Parkkonen, L. & Hämäläinen, M. (2013). "MEG and EEG data analysis with MNE-Python". In: *Frontiers in Neuroscience* 7, p. 267. DOI: 10.3389/fnins.2013.00267.

Gramfort, A. & Luessi, M. & Larson, E. & Engemann, D. A. & Strohmeier, D. & Brodbeck, C. & Parkkonen, L. & Hämäläinen, M. S. (2014). "MNE software for processing MEG and EEG data". In: *NeuroImage* 86, pp. 446–460. DOI: 10.1016/j.neuroimage.2013.10.027.

Gray, C. M. & König, P. & Engel, A. K. & Singer, W. (1989). "Oscillatory responses in cat visual cortex exhibit inter-columnar synchronization which reflects global stimulus properties". In: *Nature* 338.6213, p. 334. DOI: 10.1038/338334a0.

Gross, J. & Kujala, J. & Hämäläinen, M. & Timmerman, L. & Schnitzler, A. & Salmelin, R. (2001). "Dynamic imaging of coherent sources: Studying neural interactions in the human brain". In: *Proceedings of the National Academy of Sciences of the United States of America* 98.2, pp. 694–699. DOI: 10.1073/pnas.98.2.694.

Gross, J. & Kujala, J. & Salmelin, R. & Schnitzler, A. (2010). "Noninvasive Functional Tomographic Connectivity Analysis with MEG". In: *MEG: An Introduction to Methods*. Ed. by Hansen, P. & Kringelbach, M. & Salmelin, R. London: Oxford University Press, pp. 216–244. ISBN: 978-0-19-530723-8.

Gross, J. & Baillet, S. & Barnes, G. & Henson, R. & Hillebrand, A. & Jensen, O. & Jerbi, K. & Litvak, V. & Maess, B. & Oostenveld, R. & Parkkonen, L. & Taylor, J. & van Wassenhove, V. & Wibral, M. & Schoffelen, J.-M. (2013). "Good practice for conducting and reporting MEG research". In: *NeuroImage* 65, pp. 349–363. DOI: 10.1016/j.neuroimage.2012.10.001.

Guevara, M. A. & Corsi-Cabrera, M. (1996). "EEG coherence or EEG correlation?" In: *International Journal of Psychophysiology* 23.3, pp. 145–153. DOI: 10.1016/S0167-8760(96)00038-4.

Hauke, J. & Kossowski, T. (2011). "Comparison of values of Pearson's and Spearman's correlation coefficients on the same sets of data". In: *Quaestiones Geographicae* 30.2, pp. 87–93. DOI: 10.2478/v10117-011-0021-1.

Hillebrand, A. & Barnes, G. R. (2005). "Beamformer analysis of MEG data". In: vol. 68. Elsevier, pp. 149–171. DOI: 10.1016/S0074-7742(05)68006-3.

Horwitz, B. (2003). "The elusive concept of brain connectivity". In: *NeuroImage* 19.2, pp. 466–470. DOI: 10.1016/S1053-8119(03)00112-5.

Hämäläinen, M. & Hari, R. & Lounasmaa, O. V. & Knuutila, J. & Ilmoniemi, R. J. (1993). "Magnetoencephalography-theory, instrumentation, and applications to noninvasive studies of the working human brain". In: *Reviews of Modern Physics* 65, pp. 413–497. DOI: 10.1103/RevModPhys.65.413.

Hämäläinen, M. S. & Sarvas, J. (1989). "Realistic conductivity geometry model of the human head for interpretation of neuromagnetic data". In: *IEEE Transactions on Biomedical Engineering* 36.2, pp. 165–171. DOI: 10.1109/10.16463.

Jalava, A. (2009). "Detection of task-related neural networks with dynamic imaging of coherent sources". Master's thesis. Finland: Helsinki University of Technology.

Jas, M. & Larson, E. & Engemann, D. A. & Leppäkangas, J. & Taulu, S. & Hämäläinen, M. & Gramfort, A. (2018). "A Reproducible MEG/EEG Group Study With the MNE Software: Recommendations, Quality Assessments, and Good Practices". In: *Frontiers in Neuroscience* 12. DOI: 10.3389/fnins.2018.00530.

Jensen, O. & Hesse, C. (2010). "Estimating Distributed Representations of Evoked Responses and Oscillatory Brain Activity". In: *MEG: An Introduction to Methods*. Ed. by Hansen, P. & Kringelbach, M. & Salmelin, R. London: Oxford University Press, pp. 156–185. ISBN: 978-0-19-530723-8.

Kopell, N & Ermentrout, G. & Whittington, M. & Traub, R. (2000). "Gamma rhythms and beta rhythms have different synchronization properties". In: *Proceedings of the National Academy of Sciences of the United States of America* 97.4, pp. 1867–1872. DOI: 10.1073/pnas.97.4.1867.

Kruskal, W. H. & Wallis, W. A. (1952). "Use of Ranks in One-Criterion Variance Analysis". In: *Journal of the American Statistical Association* 47.260, pp. 583–621. DOI: 10.1080/01621459.1952.10483441.

Laaksonen, H. & Kujala, J. & Salmelin, R. (2008). "A method for spatiotemporal mapping of event-related modulation of cortical rhythmic activity". In: *NeuroImage* 42.1, pp. 207–217. DOI: 10.1016/j.neuroimage.2008.04.175.

Lessard, C. S. (2005). *Signal processing of random Physiological Signals*. Morgan & Claypool Publishers, p. 209. 232 pp. ISBN: 1-59829-039-8 (electronic), 978-1-59829-038-7 (paper).

Liljeström, M. & Kujala, J. & Stevenson, C. & Salmelin, R. (2015). "Dynamic reconfiguration of the language network preceding onset of speech in picture naming". In: *Human Brain Mapping* 36.3, pp. 1202–1216. DOI: 10.1002/hbm.22697.

Lopes da Silva, F. (2010). "Electrophysiological basis of MEG Signal". In: *MEG: An Introduction to Methods*. Ed. by Hansen, P. & Kringelbach, M. & Salmelin, R. London: Oxford University Press, pp. 1–23. ISBN: 978-0-19-530723-8.

Maris, E. & Schoffelen, J.-M. & Fries, P. (2007a). "Nonparametric statistical testing of coherence differences". In: *Journal of Neuroscience Methods* 163.1, pp. 161–175. DOI: 10.1016/j.jneumeth.2007.02.011.

Maris, E. & Oostenveld, R. (2007b). "Nonparametric statistical testing of EEG-and MEG-data". In: *Journal of Neuroscience Methods* 164.1, pp. 177–190. DOI: 10.1016/j.jneumeth.2007.03.024.

Miltner, W. H. & Braun, C. & Arnold, M. & Witte, H. & Taub, E. (1999). "Coherence of gamma-band EEG activity as a basis for associative learning". In: *Nature* 397.6718, pp. 434–436. DOI: 10.1038/17126.

Mormann, F. & Lehnertz, K. & David, P. & Elger, C. E. (2000). "Mean phase coherence as a measure for phase synchronization and its application to the EEG of epilepsy patients". In: *Physica D: Nonlinear Phenomena* 144.3-4, pp. 358–369. DOI: 10.1016/S0167-2789(00)00087-7.

Mosher, J. C. & Leahy, R. M. & Lewis, P. S. (1999). "EEG and MEG: forward solutions for inverse methods". In: *IEEE Transactions on Biomedical Engineering* 46.3, pp. 245–259. DOI: 10.1109/10.748978.

Mosher, J. C. & Baillet, S. & Leahy, R. M. (2003). "Equivalence of linear approaches in bioelectromagnetic inverse solutions". In: *IEEE Workshop on Statistical Signal Processing*. Vol. 28, pp. 294–297. DOI: 10.1109/SSP.2003.1289402.

Nijholt, A. & Tan, D. & Pfurtscheller, G. & Brunner, C. & Millán, J. d. R. & Allison, B. & Graimann, B. & Popescu, F. & Blankertz, B. & Müller, K.-R. (2008). "Brain-computer Interfacing for Intelligent Systems". In: *IEEE Intelligent Systems* 23.3, pp. 72–79. DOI: 10.1109/MIS.2008.41.

Nolte, G. & Curio, G. (1999). "The effect of artifact rejection by signal-space projection on source localization accuracy in MEG measurements". In: *IEEE Transactions on Biomedical Engineering* 46.4, pp. 400–408. DOI: 10.1109/10.752937.

Nolte, G. & Bai, O. & Wheaton, L. & Mari, Z. & Vorbach, S. & Hallett, M. (2004). "Identifying true brain interaction from EEG data using the imaginary part of coherency". In: *Clinical Neurophysiology* 115.10, pp. 2292–2307.

Oostenveld, R. & Fries, P. & Maris, E. & Schoffelen, J.-M. (2011). "FieldTrip: Open Source Software for Advanced Analysis of MEG, EEG, and Invasive Electrophysiological Data". In: *Computational Intelligence and Neuroscience* 2011. DOI: 10.1155/2011/156869.

Palva, J. M. & Palva, S. & Kaila, K. (2005). "Phase Synchrony among Neuronal Oscillations in the Human Cortex". In: *The Journal of Neuroscience* 25.15, pp. 3962–3972. DOI: 10.1523/JNEUROSCI.4250-04.2005.

Parkkonen, L. (2010). "Instrumentation and Data Preprocessing". In: *MEG: An Introduction to Methods*. Ed. by Hansen, P. & Kringelbach, M. & Salmelin, R. London: Oxford University Press, pp. 24–64. ISBN: 978-0-19-530723-8.

Penrose, R. (1955). "A generalized inverse for matrices". In: *Mathematical Proceedings of the Cambridge Philosophical Society* 51.3, pp. 406–413. DOI: 10.1017/S0305004100030401.

Purves, D. & Augustine, G. J. & Fitzpatrick, D. & Hall, W. C. & LaMantia, A.-S. & McNamara, J. O. & Williams, S. M. (2004). *Neuroscience*. 3. ed. Sunderland (Mass.): Sinauer, pp. 31–45. 773 pp. ISBN: 0-87893-725-0.

Real, R. & Vargas, J. M (1996). "The probabilistic basis of Jaccard's index of similarity". In: *Systematic Biology* 45.3, pp. 380–385. DOI: 10.1093/sysbio/45.3.380.

Rose, C. L. & Murphy, L. B. & Byard, L. & Nikzad, K. (2002). "The role of the Big Five personality factors in vigilance performance and workload". In: *European Journal of Personality* 16.3, pp. 185–200. DOI: 10.1002/per.451.

Saarinen, T. & Jalava, A. & Kujala, J. & Stevenson, C. & Salmelin, R. (2015). "Task-sensitive reconfiguration of corticocortical 6-20 Hz oscillatory coherence in naturalistic human performance". In: *Human Brain Mapping* 36.7, pp. 2455–2469. DOI: 10.1002/hbm.22784.

Salinas, E. & Sejnowski, T. J. (2000). "Impact of correlated synaptic input on output firing rate and variability in simple neuronal models". In: *Journal of Neuroscience* 20.16, pp. 6193–6209. DOI: 10.1523/JNEUROSCI.20-16-06193.2000.

Sauseng, P. & Klimesch, W. & Schabus, M. & Doppelmayr, M. (2005). "Fronto-parietal EEG coherence in theta and upper alpha reflect central executive functions of working memory". In: *International Journal of Psychophysiology* 57.2, pp. 97–103. DOI: 10.1016/j.ijpsycho.2005.03.018.

Schoffelen, J. M. & Gross, J. (2009). "Source connectivity analysis with MEG and EEG". In: *Human Brain Mapping* 30.6, pp. 1857–1865. DOI: 10.1002/hbm.20745.

Sekihara, K. & Nagarajan, S. S. & Poeppel, D. & Marantz, A. & Miyashita, Y. (2001). "Reconstructing spatio-temporal activities of neural sources using an MEG vector beamformer technique". In: *IEEE Transactions on Biomedical Engineering* 48.7, pp. 760–771. DOI: 10.1109/10.930901.

Singer, W. (1999). "Neuronal Synchrony: A Versatile Code for the Definition of Relations?" In: *Neuron* 24.1, pp. 49–65. DOI: 10.1016/S0896-6273(00)80821-1.

Smith, S. M. & Jenkinson, M. & Woolrich, M. W. & Beckmann, C. F & Behrens, T. E. & Johansen-Berg, H. & Bannister, P. R. & De Luca, M. & Drobnjak, I. & Flitney, D. E & Niazy, R. K. & Saunders, J. & Vickers, J. & Zhang, Y. & Stefano, N. D. & Brady, J. M. & Matthews, P. M. (2004). "Advances in functional and structural MR image analysis and implementation as FSL". In: *NeuroImage* 23, S208–S219. DOI: 10.1016/j.neuroimage.2004.07.051.

Srinivasan, R. & Winter, W. R. & Ding, J. & Nunez, P. L. (2007). "EEG and MEG coherence: Measures of functional connectivity at distinct spatial scales of neocortical dynamics". In: *Journal of Neuroscience Methods* 166.1, pp. 41–52. DOI: 10.1016/j.jneumeth.2007.06.026.

Sun, F. T. & Miller, L. M. & D'esposito, M. (2004). "Measuring interregional functional connectivity using coherence and partial coherence analyses of fMRI data". In: *NeuroImage* 21.2, pp. 647–658. DOI: 10.1016/j.neuroimage.2003.09.056.

Tallon-Baudry, C. & Bertrand, O. & Delpuech, C. & Pernier, J. (1997). "Oscillatory γ-band (30–70 Hz) activity induced by a visual search task in humans". In: *Journal of Neuroscience* 17.2, pp. 722–734. DOI: 10.1523/JNEUROSCI.17-02-00722.1997.

Tallon-Baudry, C. & Kreiter, A. & Bertrand, O. (1999). "Sustained and transient oscillatory responses in the gamma and beta bands in a visual short-

term memory task in humans". In: *Visual Neuroscience* 16.3, pp. 449–459. DOI: 10.1017/S0952523899163065.

Taulu, S. & Kajola, M. (2005). "Presentation of electromagnetic multichannel data: the signal space separation method". In: *Journal of Applied Physics* 97.12, pp. 1–10. DOI: 10.1063/1.1935742.

Taulu, S. & Simola, J. (2006). "Spatiotemporal signal space separation method for rejecting nearby interference in MEG measurements". In: *Physics in Medicine & Biology* 51.7, pp. 1759–1768. DOI: 10.1088/0031-9155/51/7/008.

Van Veen, B. D. & Buckley, K. M. (1988). "Beamforming: A Versatile Approach to Spatial Filtering". In: *IEEE ASSP Magazine* 5.2, pp. 4–24. DOI: 10.1109/53.665.

van Vliet, M. & Liljeström, M. & Aro, S. & Salmelin, R. & Kujala, J. (2018). "Analysis of functional connectivity and oscillatory power using DICS: from raw MEG data to group-level statistics in Python". In: *Frontiers in Neuroscience* 12.586. DOI: 10.3389/fnins.2018.00586.

Warm, J. S & Parasuraman, R. & Matthews, G. (2008). "Vigilance requires hard mental work and is stressful". In: *Human Factors* 50.3, pp. 433–441. DOI: 10.1518/001872008X312152.

Welch, P. D. (1967). "The Use of Fast Fourier Transform for the Estimation of Power Spectra: A Method Based on Time Averaging Over Short, Modified Periodograms". In: *IEEE Transactions on Audio and Electroacoustics* 15.2, pp. 70–73. DOI: 10.1109/TAU.1967.1161901.

Whalen, C. & Maclin, E. L. & Fabiani, M. & Gratton, G. (2008). "Validation of a method for coregistering scalp recording locations with 3D structural MR images". In: *Human Brain Mapping* 29.11, pp. 1288–1301. DOI: 10.1002/hbm.20465.

Yeung, A. W. K. & Goto, T. K. & Leung, W. K. (2017). "The changing landscape of neuroscience research, 2006-2015: A bibliometric study". In: *Frontiers in Neuroscience* 11.120. DOI: 10.3389/fnins.2017.00120.